

***Einstein@Home* Searches for Gamma-ray Pulsars in the Inner Galaxy**

C. J. CLARK ,^{1,2} M. DI MAURO ,³ J. WU ,⁴ B. ALLEN ,^{1,2} O. BEHNKE ,^{1,2} H. B. EGGENSTEIN ,^{1,2}
B. MACHENSCHALK ,^{1,2} L. NIEDER ,^{1,2} P. M. SAZ PARKINSON ,⁵ A. ASHOK ,^{1,2,6} P. BRUEL ,⁷
B. McGLOUGHLIN ,^{1,2} M. A. PAPA ,^{1,2} F. CAMILO ,⁸ M. KERR ,⁹ P. VORAGANTI PADMANABH ,^{1,2} AND
S. M. RANSOM 

¹Max Planck Institute for Gravitational Physics (Albert Einstein Institute), D-30167 Hannover, Germany

²Leibniz Universität Hannover, D-30167 Hannover, Germany

³Istituto Nazionale di Fisica Nucleare, Sezione di Torino, I-10125 Torino, Italy

⁴Max-Planck-Institut für Radioastronomie, Auf dem Hügel 69, D-53121 Bonn, Germany

⁵Santa Cruz Institute for Particle Physics, Department of Physics and Department of Astronomy and Astrophysics, University of California at Santa Cruz, Santa Cruz, CA 95064, USA

⁶Department of Physics, Oregon State University, Corvallis, OR 97331, USA

⁷Laboratoire Leprince-Ringuet, CNRS/IN2P3, École polytechnique, Institut Polytechnique de Paris, 91120 Palaiseau, France

⁸South African Radio Astronomy Observatory, 2 Fir Street, Observatory, 7925, South Africa

⁹Space Science Division, Naval Research Laboratory, Washington, DC 20375-5352, USA

¹⁰National Radio Astronomy Observatory, 1003 Lopezville Road, Socorro, NM 87801, USA

ABSTRACT

The *Fermi* Large Area Telescope (LAT) has revealed a mysterious extended excess of GeV gamma-ray emission around the Galactic Center, which can potentially be explained by unresolved emission from a population of pulsars, particularly millisecond pulsars (MSPs), in the Galactic bulge. We used the distributed volunteer computing system *Einstein@Home* to search the *Fermi*-LAT data for gamma-ray pulsations from sources in the inner Galaxy, to try to identify the brightest members of this putative population. We discovered four new pulsars, including one new MSP and one young pulsar whose angular separation to the Galactic Center of 0.93° is the smallest of any known gamma-ray pulsar. We demonstrate a phase-resolved difference imaging technique that allows the flux from this pulsar to be disentangled from the diffuse Galactic Center emission. No radio pulsations were detected from the four new pulsars in archival radio observations or during the MPIfR-MeerKAT Galactic Plane Survey. While the distances to these pulsars remain uncertain, we find that it is more likely that they are all foreground sources from the Galactic disk, rather than pulsars originating from the predicted bulge population. Nevertheless, our results are not incompatible with an MSP explanation for the GC excess, as only one or two members of this population would have been detectable in our searches.

1. INTRODUCTION

Observations by the Large Area Telescope (LAT) onboard the *Fermi Gamma-ray Space Telescope* (W. B. Atwood et al. 2009) have revealed an excess of GeV gamma-ray emission in the inner region of our Galaxy (first discovered by L. Goodenough & D. Hooper 2009, and recently reviewed by S. Murgia 2020). While the presence of this excess has been confirmed in multiple independent analyses (e.g., D. Hooper & L. Goodenough 2011; K. N. Abazajian & M. Kaplinghat 2012; F. Calore et al. 2015; M. Ackermann et al. 2017; M. Di Mauro 2021), which generally find the excess to be spatially extended and to have a spectrum that peaks in the GeV range, the large and uncertain fore/background flux from the interstellar medium and nearby Galactic sources makes it challenging to robustly measure its

spectral and spatial properties. As a result, the origin of this excess remains unclear.

Two main hypotheses for the origin of this Galactic Center (GC) excess have emerged. The first is that it is the signature of a central concentration of dark matter, and is produced through the annihilation of weakly-interacting massive particles (WIMPs). This hypothesis is based on the observations that the spatial distribution of the excess appears to be consistent with the generalized Navarro-Frenk-White (NFW, J. F. Navarro et al. 1996) distribution expected for dark matter, and that the shape of the spectrum can be reproduced by the annihilation of WIMPs with a mass in the plausible range of 30–300 GeV (S. Murgia 2020, and references therein).

The leading alternative to this dark-matter explanation is that the GeV excess is due to the combined emission from an unresolved, centrally concentrated population of millisecond pulsars (MSPs) numbering in the thousands or tens of thousands (e.g. K. N. Abazajian 2011; F. Calore et al. 2016; P. L. Gonthier et al. 2018;

H. Ploeg et al. 2020). It has long been predicted that such a “bulge” population of MSPs might exist in the inner Galaxy (e.g. W. Wang et al. 2005; R. S. Wharton et al. 2012; J.-P. Macquart & N. Kanekar 2015), where the larger stellar density and encounter rate encourages binary MSP formation, and where the remnants of disrupted MSP-rich globular clusters might be expected to reside (S. D. Tremaine et al. 1975). Further evidence for this population comes from the increased density of low-mass X-ray binaries (the progenitors of MSPs) at the GC (M. P. Muno et al. 2005) as well as at the center of the Andromeda galaxy (K. N. Abazajian & M. Kaplinghat 2012). The *Fermi* LAT has detected pulsed gamma-ray emission from more than 150 MSPs (D. A. Smith et al. 2023, hereafter 3PC), and these objects have characteristic curved gamma-ray spectra peaking at GeV energies, similar to that of the GC excess.

Confirming or ruling out either of these hypotheses is a crucial, although extremely challenging goal. It has not yet proved possible to distinguish between these hypotheses in the gamma-ray data alone. Both dark-matter and MSP models can reproduce the observed properties of the GC excess, within their large systematic uncertainties, and the gamma-ray spectra predicted by these models only differ significantly at low gamma-ray energies, where there are high levels of source/background confusion, and at high energies where photon counting statistics are lower (although see S. Manconi et al. 2024).

Additional observations, of other sources with similar gamma-ray emission or at other wavelengths, will likely be required to settle the debate. In the case of the dark-matter hypothesis, evidence would come from additional astrophysical detections, e.g. the discovery of similar emission from the Milky Way’s satellite dwarf spheroidal galaxies (M. Ackermann et al. 2011), or from the direct detection of dark matter particles with similar masses and cross-sections in the laboratory.

For the MSP hypothesis, searches with radio telescopes could detect individual members of this predicted “bulge” population, and with large enough numbers this could be distinguished from the known population in the Galactic disk. However, discovering new MSPs in this region of the Galaxy is particularly challenging. First, MSPs in the inner Galaxy are distant, and therefore faint; more than 97% of Galactic MSPs (excluding those in globular clusters) in the ATNF Pulsar Catalogue (R. N. Manchester et al. 2005)¹¹ are closer than the 8.2 kpc distance to the GC. Second, the dense interstellar medium in the inner Galaxy, and the resulting large column density of free electrons along that line-of-sight, means that radio emission from MSPs is scattered (spread out in time) and dispersed (delayed in time with a frequency dependence), with both of these effects mak-

ing their pulsations harder to detect. Likely as a result of these effects, only one MSP has been discovered within 1° of the GC (M. E. Lower et al. 2024), and simulations by J.-P. Macquart & N. Kanekar (2015) and F. Calore et al. (2016) predict that only a small number of MSPs from this putative bulge population may be found in the most sensitive surveys currently possible with MeerKAT¹². Discovering new MSPs in the inner Galaxy is a central goal for the MPIfR-MeerKAT Galactic Plane Survey (MMIGPS, P. V. Padmanabhan et al. 2023), which will search the GC at S-band (~ 2 –3 GHz), where the higher radio frequency helps mitigate some of the deleterious propagation effects, but it is possible that next-generation telescopes e.g. the SKA, ngVLA and DSA-2000 will be required to properly probe this predicted population (F. Calore et al. 2016).

However, the MSP hypothesis has one further property that may enable some limited tests in the gamma-ray data itself, which is that the gamma-ray emission from individual MSPs is pulsed in time. Detecting an individual gamma-ray pulsar in the *Fermi*-LAT point source at the position of the GC, 4FGL J1745.6-2859 (S. Abdollahi et al. 2020), is unlikely: under this hypothesis, this point source represents the combined emission of hundreds or even thousands of pulsars, and so a single pulsar would have to be extremely bright to stand out on top of this. The GeV excess is, however, extended, possibly up to around 10° from the GC (M. Ackermann et al. 2011; M. Di Mauro 2021), and we may therefore hope that there are rare, bright members of this population lying $\gtrsim 1^\circ$ from the GC, where they can be individually resolved above the local background flux. Gamma-ray pulsations have now been detected from individual MSPs in four globular clusters (P. C. C. Freire et al. 2011; J. H. K. Wu et al. 2013; P. Zhang et al. 2022, 2023), where a similar (albeit much smaller) background from the combined emission of other pulsars in the cluster is (likely) present. D. V. Malyshev (2024) also find that a fraction of the extended GeV excess has now been resolved into individual point sources in the latest *Fermi*-LAT data, as would be expected for a population of discrete sources.

Detecting gamma-ray pulsations from a previously unknown pulsar requires computationally-demanding searches over at least four parameters (the spin period, spin-down rate and two sky-position parameters). To make these searches computationally feasible, necessary compromises must be made which reduce their sensitivity (W. B. Atwood et al. 2006), meaning that only fairly bright isolated pulsars can be discovered in this route (we quantify this in Section 4). Nevertheless, such searches have discovered more than 80 new pulsars (e.g.,

¹¹ <https://www.atnf.csiro.au/research/pulsar/psrcat>

¹² While the FAST telescope is more sensitive, its location in the Northern Hemisphere means that it cannot observe the Galactic Center.

A. A. Abdo et al. 2009; P. M. Saz Parkinson et al. 2010; H. J. Pletsch et al. 2012a; D. A. Smith et al. 2023), including 7 new gamma-ray MSPs (C. J. Clark et al. 2018; D. A. Smith et al. 2023). Three binary MSPs have also been found using the same methods (H. J. Pletsch et al. 2012b; L. Nieder et al. 2020b; C. J. Clark et al. 2021), but these required precise constraints on their orbital parameters and sky positions through optical observations of their binary companions to account for their orbital Doppler shifts. Binary MSPs cannot yet be discovered in these searches without prior orbital constraints as the orbital parameter volume is prohibitively large. While most MSPs in the putative bulge population are likely to be in binary systems, and therefore out of reach to gamma-ray pulsation searches, there remains the potential for uncovering rare bright isolated MSPs in this region.

Motivated by the arguments above, we used the donated computing cycles from around 30,000 computing systems participating in the *Einstein@Home* distributed volunteer computing system (B. Knispel et al. 2010; B. Allen et al. 2013; H. J. Pletsch et al. 2013) to search for new gamma-ray pulsars in unidentified sources cataloged by *Fermi-LAT* Collaboration (2017, hereafter **2FIG**) and S. Abdollahi et al. (2020, hereafter **4FGL**) in the inner $40^\circ \times 40^\circ$ around the GC. These searches resulted in the discovery of four new pulsars, one of which is an isolated MSP, and another of which has the smallest angular separation of any known gamma-ray pulsar to the GC (0.93°). Similar *Einstein@Home* searches of pulsar-like **4FGL** sources elsewhere on the sky have resulted in a further 10 discoveries¹³, which will be reported in a separate paper.

This paper follows on from our previous descriptions of the *Einstein@Home* gamma-ray pulsar surveys in C. J. Clark et al. (2017, hereafter **Paper I**) and J. Wu et al. (2018). It is organized as follows: in Section 2 we describe our preparation of the *Fermi-LAT* data, the sources that we targeted, and our gamma-ray pulsation searching method; Section 3 presents the results of our pulsar searches and follow-up investigations of the newly discovered pulsars; we discuss the implications of our discoveries in Section 4, with a summary and conclusions in Section 5.

2. METHODS

2.1. Gamma-ray source selection and data preparation

The input for the *Einstein@Home* pulsation searches are lists of the arrival times of gamma-ray photons detected by the *Fermi-LAT*, with estimated arrival directions from within a small (few degrees) patch on the sky. Unlike searches for gamma-ray pulsations from known pulsars, which can detect pulsations from very

faint, even sub-threshold sources (D. A. Smith et al. 2019), our semi-coherent searches are only sensitive to pulsars that are bright enough to also be detectable as individual point sources in *Fermi-LAT* source catalogs through their time-integrated emission (see Section 4). Rather than searching over the whole sky (as is done in *Einstein@Home*'s searches for continuous gravitational waves from unknown pulsars, e.g. B. Steltner et al. 2023), we therefore target our searches at unidentified sources that have been detected through “catalog” analyses that search for point sources of emission, e.g. **4FGL** or **2FIG**.

As well as identifying gamma-ray point sources that may be pulsar candidates, these catalogs provide a model describing the spectra of all detected sources, from which we can derive photon probability weights (P. Bickel et al. 2008; M. Kerr 2011; P. Bruel 2019) that quantify the likelihood of each photon being emitted by a targeted source, as opposed to by the diffuse background, or a nearby unrelated point source. We use these to weight the contribution of each photon to our pulsation detection statistics, to suppress background photons without performing hard “cuts” that would be detrimental to sensitivity.

To obtain a list of candidate sources for our searches, we performed an updated version of the **2FIG** analysis, using the same procedure but with a longer data set described below, and identified sources from **4FGL** that were deemed to be likely pulsar candidates by a Random Forest classification, similar to that performed by P. M. Saz Parkinson et al. (2016).

For our searches of **2FIG** sources, we used the full duration of *Fermi-LAT* data that was available at the time, approximately 8.7 years, including Pass 8 P8R2 data (W. Atwood et al. 2013) between MJD 54682 (2008 August 04) and MJD 57847 (2017 April 04). This time span includes a 1-year interval¹⁴ in which *Fermi*'s observing strategy was modified to provide enhanced exposure towards the Galactic Center (J. E. McEnery et al. 2014). We used SOURCE-class photons and the P8R2_SOURCE_V6 instrument response functions (IRFs), with zenith angles smaller than 90° . Photons from the inner-most $40^\circ \times 40^\circ$ around the GC were included, split into overlapping 8° -radius circular regions in which source identification and spectral analyses were performed.

As described in **2FIG**, these analyses were performed with two different diffuse interstellar emission models: the `gll_iem_v06.fits` model, used to construct the **4FGL** catalogue (hereafter referred to as the “official” (Off.) model); and an “alternate” (Alt.) model based on that of M. Ackermann et al. (2017). We also performed analyses with two different lower energy bounds, 100 MeV and 300 MeV.

¹³ https://einsteinathome.org/gammaraypulsar/FGRP1_discoveries.html

¹⁴ <https://fermi.gsfc.nasa.gov/ssc/observations/types/exposure/>

From the results of these analyses, sources were selected as being potential pulsar candidates based on them having spectral properties consistent with the observed gamma-ray pulsar population. With the spectra modeled as exponentially-cutoff power-law ($dN/dE \propto E^{-\Gamma} \exp(-E/E_{\text{cut}})$), a source was deemed to be pulsar-like if it had spectral index $0 < \Gamma < 2$ and cutoff energy $E_{\text{cut}} < 10$ GeV. From this initial list of possible pulsar candidate sources, we selected sources from the > 100 MeV and > 300 MeV analyses that fulfilled the pulsar-candidate criteria when fit using both the Off. and Alt. models, and had similar spectra between the two analyses, as well as sources that were only selected as pulsar candidates in the > 100 MeV analysis with the Off. model.

For each source, we used `gtsrcprob` to compute photon probability weights for photons from within 5° of the estimated source position, according to the models produced by these analyses. We always used the spectral model produced by the fits using the Off. model when computing photon probability weights, unless the source was originally only identified as a pulsar candidate with the Alt. model in the original `2FIG` analysis of [Fermi-LAT Collaboration \(2017\)](#). We included as many of the highest-weighted photons as were necessary to reach 99% of the expected signal-to-noise ratio (S/N) from a source, up to a maximum of 50,000 photons per source. This limit was imposed to avoid including a large number of low-weight photons that increase the computational cost of the search, which scales with the square of the number of photons, without contributing much to the recoverable S/N, which scales with the sum of the squared photon weights (see Equation 6). The 99% expected S/N threshold was reached with fewer than 50,000 photons for half of the sources in our list, and the included photons contained at least 90% (80%) of the expected total S/N for all but seven (three) sources.

For sources from `4FGL`, we used Pass 8 P8R3 data ([W. Atwood et al. 2013](#); [P. Bruel et al. 2018](#)) up to MJD 58833 (2019 December 16), selecting `SOURCE` class photons with energies above 100 MeV and using the `P8R3_SOURCE_V2` IRFs. We first included photons from within a $20^\circ \times 20^\circ$ region around each source, and used `fermipy` ([M. Wood et al. 2017](#)) to refit the spectra of the target source and all 4FGL sources within 5° , as well as the normalisation and spectral indices of the diffuse (`gll_iem_v07.fits`) and isotropic (`iso_P8R3_SOURCE_V2_v1.txt`) background models. The resulting spectral models were then used to compute photon weights using `gtsrcprob` for photons within 5° of the target source.

Finally, we removed sources that had too few weighted photons for us to reasonably expect to detect pulsations with *Einstein@Home* (determined from the expected pulsation signal-to-noise ratio, see Section 2.2, Equation (6)).

These selection criteria resulted in a list of 55 sources to search for pulsations, which are listed in Appendix A, Table A1. Some of these were searched using two or three different sets of photon weights resulting from the different spectral analyses described above (i.e. using the `2FIG` > 100 MeV, `2FIG` > 300 MeV or `4FGL` sky models) to attempt to mitigate the risk of missing a new pulsar due to using photon weights computed from an inaccurate sky model.

For sources in which we detected significant gamma-ray pulsations, we produced extended *Fermi*-LAT data sets, covering data up to MJD 60595 (2024 October 12). These were prepared using the `P8R3_SOURCE_V3` IRFs ([P. Bruel et al. 2018](#)), using the energy-dependent angular and PSF (point spread function) event-type cuts described in `4FGL`. We computed photon weights using the spectral and spatial model from [J. Ballet et al. \(2023, hereafter 4FGL-DR4\)](#), with the rescaled `gll_iem_v07` interstellar emission model associated to the 4FGL-DR4 catalog, and `iso_P8R3_SOURCE_V3_v1.txt` isotropic background model.

2.2. Gamma-ray pulsation searches

We searched these sources for gamma-ray pulsations using the methods described in [Paper I](#). These methods are similar to the “time-differencing” technique developed by [W. B. Atwood et al. \(2006\)](#), but incorporate additional techniques developed to search for continuous gravitational waves from spinning neutron stars in LIGO data ([R. Balasubramanian et al. 1996](#); [B. J. Owen 1996](#); [H. J. Pletsch & B. Allen 2009](#); [H. J. Pletsch 2011](#)) and radio pulsars ([S. M. Ransom et al. 2002](#)). Detailed descriptions of these methods can be found in [H. J. Pletsch & C. J. Clark \(2014\)](#) and [L. Nieder et al. \(2020a\)](#), which we briefly summarize here.

Describing the rotational history of an isolated gamma-ray pulsar in the *Fermi*-LAT data requires an ephemeris ($\vec{\lambda}$) containing a minimum of four parameters: the spin frequency (f), the spin-frequency derivative (\dot{f}), and two positional parameters, which we take here to be the equatorial Right Ascension (α) and Declination (δ).

In our searches, we use a simple constant spin-down phase model,

$$\phi(t; \vec{\lambda}) = f(t_{\text{SSB}}(t, \alpha, \delta) - t_{\text{ref}}) + \frac{1}{2} \dot{f} (t_{\text{SSB}}(t, \alpha, \delta) - t_{\text{ref}})^2, \quad (1)$$

where t_{ref} is a reference epoch chosen to be close to the center of the data span, and $t_{\text{SSB}}(t, \alpha, \delta)$ is the estimated time that a photon detected by the LAT at time t , propagating from a source at position (α, δ) , would have arrived at the Solar-System Barycenter (SSB, an approximately “fixed” point at the center of the Solar System). The conversions between t and t_{SSB} are known as “barycentering” corrections (with absolute values less

than $\sim (1 \text{ AU}/c) \approx 500 \text{ s}$, and are required here to account for the position-dependent Doppler shift due to *Fermi*'s orbit around the Earth, and the Earth's orbit through the Solar System (the Roemer delay), as well as much smaller general relativistic corrections for the Einstein delay ($\lesssim 2 \text{ ms}$) and Solar Shapiro delay ($\lesssim 100 \mu\text{s}$) (e.g. R. T. Edwards et al. 2006).

Pulsation strength in a set of N weighted photon arrival times, for a given ephemeris $\vec{\lambda}$, is often quantified by the H -test (O. C. de Jager et al. 1989; M. Kerr 2011),

$$H(\vec{\lambda}) = \max_{M < 20} \left[4 - 4M + \sum_{n=1}^M \mathcal{P}_n(\vec{\lambda}) \right] \quad (2)$$

which is a maximised sum over the harmonic Fourier powers, \mathcal{P}_n ,

$$\mathcal{P}_n(\vec{\lambda}) = \frac{2}{\sum_j w_j^2} \left| \sum_{j=1}^N w_j e^{-2\pi i n \phi(t_j; \vec{\lambda})} \right|^2, \quad (3)$$

where w_j is the probability weight for the j -th photon, and t_j is its LAT arrival time.

In our searches, none of the four ephemeris parameters are known precisely enough in advance to detect pulsations, and must therefore be searched over. We fill this 4-dimensional parameter space with a grid of search locations, whose density depends strongly on the length of the data (we need to be more precise in each parameter to accurately track the pulsar's rotation over longer periods of time).

An optimal spacing for this grid can be computed from the “parameter space metric” (R. Balasubramanian et al. 1996; B. J. Owen 1996), which predicts how much signal power will be lost due to a grid point not lying exactly at the true ephemeris parameters. This metric can then be used to construct a grid that minimises the average loss in S/N for a given computing budget, to maximise the probability of detecting a signal (B. Allen 2021). For gamma-ray pulsation searches, this metric is derived in H. J. Pletsch & C. J. Clark (2014) and L. Nieder et al. (2020a).

However, a grid dense enough to search for unknown pulsars in typical unidentified *Fermi*-LAT sources with arcminute positional uncertainties using the H -test, or even the Fourier power in a single harmonic, is computationally infeasible. Instead, we trade sensitivity for computational efficiency by employing a “semi-coherent” detection statistic,

$$S_T(\vec{\lambda}) = \frac{1}{\kappa_{S_T}} \sum_{j=1}^N \sum_{\substack{k=1 \\ k \neq j}}^N w_j w_k e^{-2\pi i [\phi(t_j; \vec{\lambda}) - \phi(t_k; \vec{\lambda})]} W_T(t_j - t_k), \quad (4)$$

where κ_{S_T} is a normalizing term, and $W_T(\tau)$ is a “lag window”

$$W_T(\tau) = \begin{cases} 1 & \text{for } |\tau| < T/2 \\ 0 & \text{otherwise} \end{cases}, \quad (5)$$

that only accepts photon pairs that are separated by less than half the “coherence time” T . The effect of this lag window is that the S/N is reduced, but our search only requires the phase model to be accurate over short time scales T , rather than over the entire data span T_{obs} , meaning we can use a much sparser grid of search locations. In the limit where $T = T_{\text{obs}}$, the statistic becomes the coherent Fourier power, $S_{T_{\text{obs}}}(\vec{\lambda}) = (\mathcal{P}_1(\vec{\lambda}) - 2)/2$.

For these searches, we used a coherence time of $T = 2^{22} \text{ s} \approx 48.5 \text{ d}$, twice as long as that used in Paper I. Our search grid had a maximum “mismatch” (fractional loss in S/N due to an offset in parameter space) of 15% in each dimension. We searched two regions of parameter space: one covering the majority of the known ranges of spin parameters for young pulsars, with $f < 88 \text{ Hz}$ and $-\dot{f} < 10^{-10} \text{ Hz s}^{-1}$; and another for MSPs with $88 \text{ Hz} < f < 1512 \text{ Hz}$ and $-\dot{f} < 10^{-13} \text{ Hz s}^{-1}$. These regions were conservatively chosen to also be sensitive to the second harmonic of nearly all of the fastest spinning pulsars of each category. We searched circular sky regions around each source, with radii 50% larger than the semi-major axis of the 95% confidence region from the spectral analyses.

This parameter space was split into many “work units”, each of which could be processed by a typical personal computer within a few hours, which were then distributed to the *Einstein@Home* volunteer computers. At the end of each work unit, the ten candidates with the highest detection statistic values from the semi-coherent search were automatically followed-up with refined grids and more sensitive statistics: first a semi-coherent refinement with $T = 2^{23} \text{ s}$, followed by a fully-coherent search using \mathcal{P}_1 . The ten candidates from the initial semi-coherent search, and the ten best candidates from the coherent follow-up stages were reported back to the central *Einstein@Home* servers. The most significant candidates from each source were then further refined on the ATLAS cluster¹⁵ (C. Aulbert & H. Fehrmann 2008), first using \mathcal{P}_1 with a smaller mismatch, and then using the H -test, summing up to $M \leq 5$ harmonics. At this stage we additionally computed the H -test with $f \rightarrow f/2$ and $\dot{f} \rightarrow \dot{f}/2$, in case the second harmonic had been misidentified as the fundamental spin frequency, which can happen for pulsars with double-peaked pulse profiles, since for these pulsars $\mathcal{P}_2 > \mathcal{P}_1$.

Before launching our searches, we used the photon weights to estimate in advance if it would be possible to detect pulsations from each source, to avoid wasting computing time on sources that were too faint. As we

¹⁵ <https://www.aei.mpg.de/atlas>

argued in [Paper I](#) (Appendix A) and [L. Nieder et al. \(2020a\)](#) (Section 2.5), the expected semi-coherent spectral S/N,

$$\theta_S^2 = p^2 |\gamma|^2 \sqrt{\sum_{j=1}^N \sum_{\substack{k=1 \\ k \neq j}}^N w_j^2 w_k^2 W_T(t_j - t_k)} \quad (6)$$

where γ is the Fourier coefficient of the strongest harmonic of the pulse profile (usually corresponding to the fundamental spin period, but sometimes the second harmonic for pulsars whose pulse profiles have two similar peaks separated by half a rotation) and p is the fraction of photons from the target source that are pulsed. Given a set of photon weights from a target source, and with an assumed pulse profile shape, we can therefore estimate the pulsed fraction necessary for our search to detect pulsations above a certain S/N threshold. Gamma-ray pulsars tend to have $p \approx 1$, but this fraction can appear to be smaller or even larger than unity in the presence of mis-modeled background sources that manifest as inaccurate photon weights. We choose optimistic assumptions to make this selection conservative: we took $|\gamma| = 1$, corresponding to the narrowest possible pulse profile (a delta function), and included sources where $\theta_S^2 = 8$ (approximately the threshold required for a source to reach the more sensitive coherent follow-up stages in our search) could be reached with $p \leq 1$. The estimated minimum detectable pulsed fraction for each source is listed in [Table A1](#).

3. RESULTS

We identified four new gamma-ray pulsars in the candidate lists returned by *Einstein@Home* volunteer computers. In [Section 3.5](#) we describe each of these pulsars in turn, and present the results of follow-up analyses that are described in the next few sections.

These pulsars were all clear outliers in our list of candidate H -tests (all had $H > 180$, while the most significant candidate that we do not believe to be a real pulsar signal had $H = 131$). In previous searches we have also identified pulsars that only appeared in the semi-coherent search stages, due to e.g. timing noise or glitches that prevented their power accumulating as expected in the coherent searches. We therefore manually folded and attempted to refine the parameters of marginal outlying semi-coherent candidates, but did not identify any new pulsars in this way here.

After we began our search, two new radio MSPs, PSR J1624–39¹⁶ and PSR J1730–0359 ([J. Fang et al. 2025](#)), were discovered in sources in our target list, 4FGL J1624.3–3952 and 4FGL J1730.4–0359, respectively, while ten more have likely associations with active

galactic nuclei, supernova remnants or pulsar wind nebulae, or radio/X-ray sources of unknown type listed in [4FGL-DR4](#). We note these associations in [Table A1](#). The other 40 sources remain unassociated with any known gamma-ray emitting sources detected at other wavelengths.

While we provide an estimate for the minimum pulsed fraction that each source would need to have to be detectable in our survey in [Table A1](#), we caution against interpreting these as upper limits on pulsations, as these estimates come with several caveats. First, there are types of pulsars that would not be detectable in our searches, despite being brighter than these thresholds. Most notably, we cannot detect pulsars in binary systems, which includes the majority of MSPs due to the recycling process through which they form, as the orbital Doppler shift makes our assumed phase model inapplicable. While our semi-coherent detection statistic provides some robustness to timing noise and small glitches from young pulsars, these phenomena can also greatly reduce our sensitivity to pulsations. Second, the photon weights themselves may also be inaccurate due to source confusion or unmodeled sources near the targeted sources, and this can bias our estimated thresholds. Finally, while we search a conservatively large range of sky positions around each target source, confusion between sources in the Galactic plane can cause the source position to be inaccurate, putting the true pulsar position outside our search region (e.g. [C. J. Clark et al. 2015](#)). While our searches can positively identify some sources as being gamma-ray pulsars, these caveats mean that we cannot confidently determine that a source is *not* a gamma-ray pulsar.

3.1. Gamma-ray Pulsation Timing

We performed a timing analysis using the 16-year *Fermi*-LAT data set for all four newly discovered gamma-ray pulsars to precisely estimate their rotational and astrometric parameters. These analyses followed the methods used in [Paper I](#), in which the timing parameters are varied in a Markov-Chain Monte-Carlo (MCMC) process, to maximise the pulsation likelihood according to a template pulse profile ([P. S. Ray et al. 2011](#)). For this work, we included the extension to these methods from [L. Nieder et al. \(2019\)](#), in which the parameters of the template pulse profile are also varied within the MCMC process, to marginalise over this source of uncertainty. We modeled the pulse profiles as a weighted sum of wrapped Gaussian peaks, with the number of components chosen to minimise the Bayesian Information Criterion ([G. Schwarz 1978](#)).

Two pulsars in this work, PSR J1736–3422 and PSR J1748–2815, had significant timing noise, i.e. their rotational phase significantly deviates from the constant linear spin-down model of [Equation 1](#). Timing noise is common to all known types of pulsars, and is typically well-described by a noise process with a steep “red” (i.e.,

¹⁶ <https://www.astro.umd.edu/~eferrara/pulsars/GalacticMSPs.txt>

larger amplitude at lower frequencies) power-law spectrum (e.g. W. Coles et al. 2011; M. Kerr et al. 2015; A. Parthasarathy et al. 2019). Because timing noise generally increases with spin period and spin-down rate (R. M. Shannon & J. M. Cordes 2010), it is usually not detectable in gamma-ray timing data for MSPs (FERMI-LAT Collaboration et al. 2022) and older non-recycled pulsars. We model timing noise in these pulsars as a stochastic noise process on top of a cubic spin-down model (i.e., adding the next term, $f(t - t_{\text{ref}})^3/6$ to Equation 1). We use a reduced-rank Fourier basis for this noise model, and include the corresponding Fourier coefficients as timing model parameters, with amplitudes constrained by applying a prior following a noise model spectrum whose parameters (“hyperparameters”) we also fit for. This method is similar to the “photon-by-photon” timing method of FERMI-LAT Collaboration et al. (2022), although here we perform the fitting using the Gibbs sampling method used in T. Thongmeearkom et al. (2024).

We model these noise processes using a power-law model with a low-frequency cutoff, with power spectra

$$S(f) = \frac{A^2}{12\pi^2} \left(\frac{f_c}{1 \text{ yr}^{-1}} \right)^{-\gamma} \left(1 + \left(\frac{f}{f_c} \right)^2 \right)^{-\gamma/2} \text{ yr}^3, \quad (7)$$

parameterized by the amplitude A at a reference frequency of 1 yr^{-1} , a corner frequency f_c and a spectral index γ . We applied log-uniform priors on A and $0.1/T_{\text{obs}} < f_c < 10/T_{\text{obs}}$, and a uniform prior on $0.5 < \gamma < 15$.

Our gamma-ray timing solutions are given in Table 1, and we include ephemerides compatible with the `tempo2` (R. T. Edwards et al. 2006) and `PINT` (J. Luo et al. 2018) software as supplementary material. The resulting photon phases and weighted pulse profiles are shown in Figure 1.

3.2. Radio follow-up searches

Targeting unidentified *Fermi*-LAT gamma-ray sources with radio telescopes is an efficient survey scheme for discovering new MSPs (P. S. Ray et al. 2012). As such, many sources in our target list have already undergone sensitive searches for radio pulsations (e.g., E. D. Barr et al. 2013; S. Sampa-Arsa 2016; B. Bhattacharyya et al. 2021; C. J. Clark et al. 2023; M. Kerr et al. 2025). The ephemerides that we obtain through gamma-ray timing allow us to fold radio data to search for pulsations from new gamma-ray pulsars, including in archival observations where we can now achieve higher sensitivity than in the original searches performed when the spin periods were unknown. Nevertheless, follow-up searches for radio pulsations from gamma-ray discovered pulsars have had a low detection rate (J. Wu et al. 2018; D. A. Smith et al. 2023; R. Ding et al. 2025), likely reflecting the fact that pulsars’ gamma-ray beams are observable

from a wide range of viewing angles than the comparatively narrow radio cones (e.g. C. Kalapotharakos et al. 2023).

The inner Galaxy is also being extensively studied at radio wavelengths, notably at high sensitivity and angular resolution with MeerKAT by MMGPS (P. V. Padmanabhan et al. 2023), the SARAO MeerKAT Galactic Plane Survey (SMGPS, S. Goedhart et al. 2024) and the MeerKAT legacy survey of the Galactic Center (I. Heywood et al. 2022). Each of these surveys provides imaging data from which we can place sensitive upper limits on the presence of a radio counterpart to our gamma-ray MSPs based on time-integrated flux.

MMGPS also includes pulsar search observations in three different frequency bands (UHF at 544–1088 MHz, *L*-band at 856–1712 MHz, and *S*1 at 1968–2843 MHz). Data volumes from MMGPS pulsar search observations are too high for archival storage, so we are unable to fold previous *L*-band observations of these sources. However, during the UHF and *S*-band observations, summarised in Table 2, we formed dedicated coherent tied-array beams on the best-fitting gamma-ray timing positions for these pulsars, using 40 of the 44 antennas in MeerKAT’s 1 km core.

For all pulsar-mode observations, we first cleaned the data of radio-frequency interference (RFI) using either `filtool` (Y. Men et al. 2023) for Murriyang and MeerKAT observations, or `rfifind` (S. Ransom 2011) for GBT observations, and then folded and searched the cleaned data over DMs using `dspsr` (W. van Straten & M. Bailes 2011) and `pdmp` (W. van Straten et al. 2012) (Murriyang/MeerKAT) or `prepfold` (GBT), maintaining full frequency resolution. We searched a range of DMs from 0 pc cm^{-3} up to twice the maximum DM predicted for that line-of-sight by the NE2001 (J. M. Cordes & T. J. W. Lazio 2002) and YMW16 (J. M. Yao et al. 2017) Galactic electron density models.

No radio counterparts were detected for any of the new pulsars. We summarize both the archival and new radio observations that have been performed towards our newly detected gamma-ray pulsars in Table 2. For pulsar-mode observations, we estimate upper limits on the flux density using the pulsar radiometer equation (D. R. Lorimer & M. Kramer 2004), assuming a detection threshold at $\text{S/N} = 8$, and that 70% of the bandwidth is usable after accounting for RFI and receiver roll-off. We assumed fractional pulse duty cycles of $W = 0.015\sqrt{f/(1 \text{ Hz})}$ (M. Kramer et al. 1998), up to a maximum of $W = 0.1$ for the MSP J1649–3012, where the flux density upper limit scales like $\sqrt{W/(1 - W)}$. We take the sky temperature from the 408 MHz all-sky map of C. G. T. Haslam et al. (1982), reprocessed by M. Remazeilles et al. (2015), and assume it has a power-law spectrum with spectral index -2.6 . We estimate the flux density upper limit by integrating a nominal power-law pulsar spectrum with index -1.8 (A. Karastergiou et al. 2024) and the sky temperature spectrum over the ob-

Table 1. Gamma-ray timing solutions for newly discovered pulsars

Parameter	PSR J1649–3012	PSR J1736–3422	PSR J1742–3321	PSR J1748–2815
Timing parameters				
Data span (MJD)	56265.0	56265.0	54681–60595	56265.0
Reference epoch for spin frequency, t_{ref}	56265.0	—	—	—
Reference epoch for astrometry	—	—	DE405	—
Solar system ephemeris	—	—	TDB	—
Time scale	—	—	—	—
Measured properties ^a				
R.A. (J2000), α	16 ^h 49 ^m 46 ^s 3164(8)	17 ^h 36 ^m 10 ^s 90(2)	17 ^h 42 ^m 11 ^s 58(3)	17 ^h 48 ^m 31 ^s 02(1)
Decl. (J2000), δ	−30°12'21.21(6)	−34°22'22(1)''	−33°21'21(2)''	−28°15'17(2)''
Proper motion in R.A., $\mu_\alpha \cos \delta$ (mas yr ^{−1})	−5(2)	—	—	—
Proper motion in Decl., μ_δ (mas yr ^{−1})	7(11)	—	—	—
Spin frequency, f (Hz)	292.01728830687(4)	2.882409743(3)	6.9780401641(1)	9.9843315485(4)
Spin-frequency derivative, \dot{f} (Hz s ^{−1})	−1.1264(3) $\times 10^{-15}$	−5.4428(2) $\times 10^{-13}$	−6.1822(3) $\times 10^{-14}$	−3.52083(8) $\times 10^{-13}$
Second frequency derivative \ddot{f} (Hz s ^{−2})	—	6(3) $\times 10^{-25}$	—	−2.4(6) $\times 10^{-25}$
Glitch epoch, t_g (MJD)	—	—	57401(19)	—
Glitch frequency increment, Δf_g^g (Hz)	—	—	1.48(5) $\times 10^{-8}$	—
Glitch spin-down increment, $\Delta \dot{f}_g^g$ (Hz)	—	—	−2.0(4) $\times 10^{-17}$	—
Timing noise parameters ^b				
Amplitude, $\log_{10} A$	—	−10.8 ^{+0.7} _{−1.2}	—	−10.2 ^{+0.7} _{−1.1}
Corner frequency, $\log_{10} \left(\frac{f_c}{1 \text{ yr}^{-1}} \right)$	—	< −0.8	—	< −0.2
Spectral index γ	—	> 6.0	—	> 2.8
Amplitude of 2nd component, $\log_{10} A_2$	—	−8.1 ^{+0.3} _{−0.2}	—	—
Corner frequency of 2nd component $\log_{10} \left(\frac{f_c}{1 \text{ yr}^{-1}} \right)$	—	0.3 ^{+0.1} _{−0.1}	—	—
Derived quantities ^c				
Galactic longitude, l (°)	−8.042	−5.675	−4.149	0.913
Galactic latitude, b (°)	19.207	−1.177	−1.691	−0.190
Spin period, P (ms)	3.4244547841603(5)	346.9319386(3)	143.306713130(2)	100.15893040(4)
Spin-down rate, \dot{P}	1.3209(3) $\times 10^{-20}$	6.5511(3) $\times 10^{-14}$	1.26963(6) $\times 10^{-15}$	3.53190(8) $\times 10^{-15}$
Characteristic age, τ (yr)	4 $\times 10^9$	8.4 $\times 10^4$	1.8 $\times 10^6$	4.5 $\times 10^5$
Spin-down luminosity, \dot{E} (erg s ^{−1})	1.3 $\times 10^{34}$	6.2 $\times 10^{34}$	1.7 $\times 10^{34}$	1.4 $\times 10^{35}$
Surface B -field strength, B_S (G)	2 $\times 10^8$	4.82 $\times 10^{12}$	4 $\times 10^{11}$	6 $\times 10^{11}$
Light-cylinder B -field strength, B_{LC} (G)	5 $\times 10^4$	1 $\times 10^3$	1 $\times 10^3$	6 $\times 10^3$

^aFree parameters from our gamma-ray timing model, with 1σ uncertainties on the final digits quoted in brackets

^bSince these timing noise hyperparameters typically have non-Gaussian posterior distributions, we quote 95% confidence intervals, or 95% confidence limits when an upper or lower bound cannot be determined from the data.

^cDue to the uncertain distances to these pulsars, we do not correct derived parameters for the Shklovskii effect or for relative acceleration in the Galactic potential. These effects are negligible for the three young pulsars, but are large and uncertain for the MSP J1649–2013 (see Figure 3).

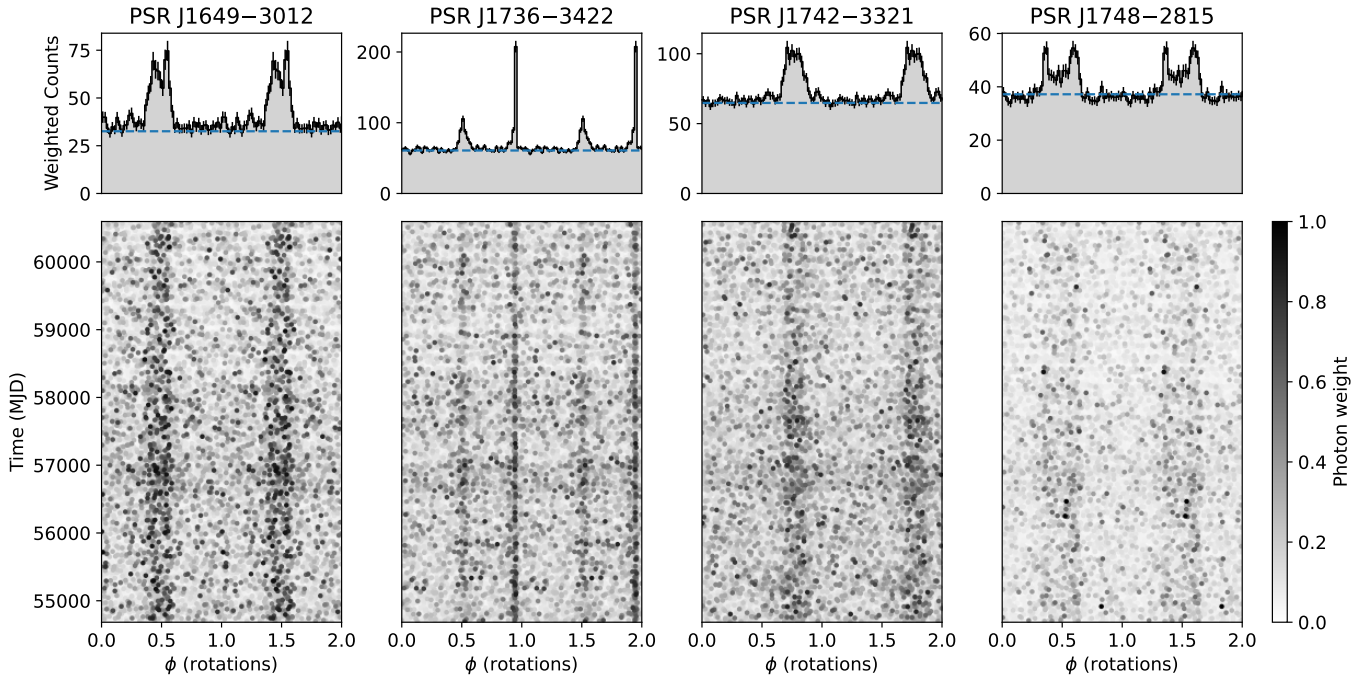


Figure 1. Photon phases and pulse profiles for the new gamma-ray pulsars discovered in this work. Lower panels show the phases for individual photons according to our best-fitting gamma-ray timing models, with the photon probability weights indicated by the grayscale. Upper panels show the integrated pulse profiles. The dashed blue lines show the estimated background level, calculated from the photon weights as $\sum_j w_j(1 - w_j)/N_{\text{bins}}$ (A. A. Abdo et al. 2013). Flux below these lines is attributed to the diffuse background or other nearby point sources. The period of enhanced exposure towards the Galactic Center is visible here as darker bands containing more photons between MJDs 56600 and 57000.

serving bandwidth, and report the flux density limit at both the central observing frequency and extrapolated to a nominal frequency of 1400 MHz.

The positions of two new pulsars, PSRs J1736–3422 and J1748–2815 were covered by MeerKAT imaging surveys, shown in Figure 2. No significant point sources consistent with the gamma-ray timing positions are detected in these images. We estimated the RMS noise level from $1' \times 1'$ regions around the gamma-ray timing positions of each pulsar, after iteratively removing pixels that were above the 3σ level. We find 2σ continuum flux density upper limits of $39 \mu\text{Jy}$ and $53 \mu\text{Jy}$ for PSRs J1736–3422 and J1748–2815, respectively, similar to the most sensitive 1400 MHz pulsed flux density upper limits for these pulsars ($30 \mu\text{Jy}$ and $56 \mu\text{Jy}$, respectively).

3.3. Searches for Continuous Gravitational Waves

The original motivation for the *Einstein@Home* project was to carry out broad searches for continuous gravitational waves. Later, the *Einstein@Home* searches were extended to search for new pulsars in radio and gamma-ray data. In turn, discoveries from these searches can be used for gravitational wave searches.

Gravitational wave emission is expected by non-axisymmetric neutron stars (e.g., P. R. Brady et al. 1998) with the dominant signal frequency being equal to twice the rotational frequency of the star ($f_{\text{GW}} = 2f$). The ephemerides obtained from gamma-ray timing can be used to construct the gravitational wave search templates. If the gamma-ray timing solutions cover all epochs of the aLIGO observing runs, fully-coherent targeted searches can be executed, which yield maximum sensitivity.

We search for such signals using data from the first, second and third observing runs of the aLIGO detectors (R. Abbott et al. 2021, 2023) from both PSRs J1649–3012¹⁷ and J1748–2815 as both objects are expected to produce signals within the detector band.

We use two distinct analysis procedures which yield similar results. The first is a frequentist approach, based on the multi-detector maximum-likelihood \mathcal{F} -statistic (C. Cutler & B. F. Schutz 2005). The second is a Bayesian \mathcal{F} -statistic-based approach detailed by A. Ashok et al. (2024). Both methods coherently combine data from the Hanford and Livingston aLIGO detectors.

The results are consistent with a non-detection. At twice the rotational frequency, we set the \mathcal{F} -statistic 95% confidence upper limits on the intrinsic gravitational wave amplitude h_0 and the corresponding Bayesian 95% credible interval upper limits on the intrinsic amplitudes, summarized in Table 3.

¹⁷ A preliminary search for this pulsar was presented in A. Ashok (2023). In this paper we present search results using an updated timing solution.

Additionally, since the gravitational wave emission may be mismatched from twice the rotational frequency, we performed an \mathcal{F} -statistic search in a band $\Delta f_{\text{GW}} = 4 \times 10^{-3} \times f_{\text{GW}}$ around each pulsar and likewise for the spindown f consistent with previous searches (R. Abbott et al. 2022; A. Ashok et al. 2021). The search was divided into multiple 10-mHz wide sub-bands and upper limits on h_0 are set in each band. We obtain a mean upper limit value of h_0 across all 10-mHz bands of 2.6×10^{-26} and 6.2×10^{-25} for J1649–3012 and J1748–2815 respectively, larger values than the targeted search upper limits due to the “trials factor” effect of searching over many waveform templates. We find no evidence of gravitational wave emission in these additional extended parameter space searches as the maximum \mathcal{F} -statistic value in each band is consistent with Gaussian noise.

Our upper limits on h_0 can be expressed as upper limits on the ellipticity ϵ of the pulsars (B. P. Abbott et al. 2019). This is,

$$\epsilon = 2.36 \times 10^{-6} \times \left(\frac{h_0}{10^{-25}} \right) \left(\frac{10^{45} \text{ g cm}^2}{I_{zz}} \right) \times \left(\frac{100 \text{ Hz}}{f_{\text{rot}}} \right)^2 \left(\frac{d}{1 \text{ kpc}} \right), \quad (8)$$

where I_{zz} is the moment of inertia about the spin axis, d is the distance to the pulsar and f_{rot} is the rotational frequency. The ellipticity upper limits can be calculated as a function of distance to the pulsar. The calculated ellipticity upper limit values as a function of distance, using the frequentist upper limits on the intrinsic gravitational wave amplitude and the canonical value of $I_{zz} = 10^{45} \text{ g cm}^2$ are shown in Table 3.

It was possible albeit unlikely that our searches would have detected a gravitational wave. How likely these searches would have yielded a detection and the physical significance of our results can be assessed by taking the ratio between our measured gravitational wave amplitude upper limits and the theoretical maximum “spindown limit” gravitational wave amplitude h_0^{spdwn} ; that is the gravitational wave amplitude produced by the pulsar assuming that all of the rotational energy was channeled into gravitational wave emission. If $h_0^{95\%}/h_0^{\text{spdwn}}$ is less than 1, then the upper limits are informative. Assuming the most optimistic case in which each pulsar is located at the minimum possible distance of 1 kpc from Earth (see next subsection), we compute h_0^{spdwn} . The corresponding results using the frequentist upper limits are shown in Table 3.

3.4. Estimating gamma-ray pulsar distances

Distances for new pulsars are typically estimated by comparing the radio dispersion measure to the line-of-sight electron column density predicted by the NE2001 (J. M. Cordes & T. J. W. Lazio 2002) and YMW16

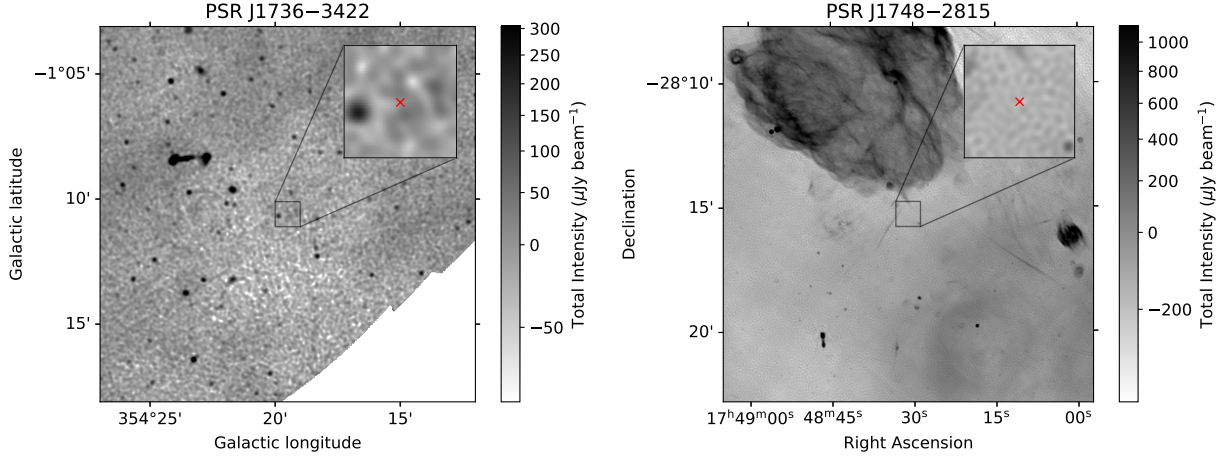


Figure 2. MeerKAT radio images at 1.28 GHz covering the locations of two new gamma-ray pulsars. No plausible radio counterparts are detected. Left panel: cutout from the SARA0 MeerKAT Galactic Plane Survey (S. Goedhart et al. 2024) covering the position of PSR J1736–3422. Right panel: cutout from the MeerKAT Galactic Center Mosaic (I. Heywood et al. 2022) covering the position of PSR J1748–2815. Inset panels contain the $1' \times 1'$ region around the pulsars from which we estimated the RMS noise level to obtain flux-density upper limits, with the gamma-ray timing positions of the pulsars marked by red crosses. The positional uncertainties are smaller than these markers. The grayscale has the mean intensity subtracted, and a square-root normalisation applied, as indicated on the color bar.

Table 2. Radio pulsar search observations of newly-discovered pulsars

Pulsar	Telescope	Receiver/Backend	Epoch	Duration	Frequency	Max. DM	S_{avg}^a	S_{1400}^b
			(MJD)	(min)	(MHz)	(pc cm $^{-3}$)	(μJy)	(μJy)
J1649–3012	GBT	UHF/GUPPI	56725.5322	45	720–920	400	< 53	< 20
	Murriyang	H-OH/PDFB4	57697.2094	60	1241–1497	400	< 87	< 84
	GBT	UHF/GUPPI	57781.5783	30	720–920	400	< 65	< 25
	MeerKAT	UHF/FBFUSE	60664.2180	8	544–1088	400	< 91	< 35
J1736–3422	MeerKAT	S1/FBFUSE	60660.2534	20	1968–2843	2300	< 11	< 30
	MeerKAT	UHF/FBFUSE	60664.2334	8	544–1088	2300	< 85	< 32
J1742–3321	MeerKAT	UHF/FBFUSE	60664.2395	8	544–1088	3000	< 100	< 38
J1748–2815	Murriyang	UWL/Medusa	59021.6701	3×10.25	704.5–4031.5	3000	< 25	< 65
	Murriyang	UWL/Medusa	59046.6033	3×10.25	704.5–4031.5	3000	< 25	< 65
	MeerKAT	S1/FBFUSE	60660.2370	20	1968–2843	3000	< 21	< 56
	MeerKAT	UHF/FBFUSE	60664.2274	8	544–1088	3000	< 307	< 116

^aFlux density upper limit at the central observing frequency, assuming a power-law pulsar spectrum with index -1.8 , and a sky-temperature spectrum with index -2.6 .

^bFlux density upper limit, extrapolated to a reference frequency of 1400 MHz.

Table 3. Continuous Gravitational Wave Upper Limit Results

Pulsar	f_{GW} [Hz]	$h_0^{95\%}$	$h_0^{95\%}$ (Bayes.)	$h_0^{\text{spdwn}} \times (d/1\text{kpc})$	$\epsilon^{95\%} \times (1\text{kpc}/d)$	$h_0^{95\%}/h_0^{\text{spdwn}}$ (at $d = 1\text{kpc}$)
J1649–3012	≈ 584.03	5.5×10^{-27}	4.2×10^{-27}	1.6×10^{-27}	1.5×10^{-8}	3.4
J1748–2815	≈ 19.97	1.2×10^{-25}	1.0×10^{-25}	1.5×10^{-25}	2.8×10^{-4}	0.8

(J. M. Yao et al. 2017) models. However, most pulsars discovered in gamma-ray searches appear to be “radio quiet”, and this includes all four of the new pulsars discovered here.

In the absence of a radio detection and resulting dispersion measure, we can only crudely estimate the distance to the new pulsars by using the measured gamma-ray fluxes and appealing to the estimated spin-down power budget. In 3PC, the gamma-ray efficiencies $\eta = L_\gamma/\dot{E}$ implied by the distances (d), gamma-ray luminosities (L_γ) and spin-down powers ($\dot{E} = 4\pi^2 I_{zz} f \dot{f}$, for an assumed moment of inertia $I_{zz} = 10^{45} \text{ g cm}^2$) of the population of gamma-ray MSPs were found to lie within the range $0.01 \lesssim \eta \lesssim 1$. C. Kalapotharakos et al. (2023) found that pulsars’ gamma-ray beams sweep out a non-isotropic pattern on the sky in which most viewing angles receive more flux than they would if emission was isotropic, meaning that efficiencies calculated under the assumption of isotropic emission are usually over-estimates. This also means that apparent efficiencies $\eta > 1$ are possible, but no pulsar in 3PC was found to significantly exceed this level, so we use this as an approximate upper limit on possible luminosities. Motivated by gamma-ray emission models that predict $L_\gamma \propto \dot{E}^{1/2}$ (J. Arons 1996), a “heuristic” efficiency, $\eta_h = (\dot{E}/10^{33} \text{ erg s})^{-1/2}$ has been found to provide a reasonable prediction for the majority of the gamma-ray pulsar population (3PC). For the four new pulsars found here, these heuristic efficiencies range from 10% to 30%. We therefore use the observed gamma-ray fluxes from 4FGL-DR4 and these typical efficiencies to estimate likely and maximum distances to the new pulsars.

3.5. New Pulsars

In the following sections we give individual details and results from our follow-up investigations of the newly-discovered gamma-ray pulsars.

3.5.1. PSR J1649–3012

With a spin period of 3.4 ms, this is the third isolated MSP to be found by *Einstein@Home* (C. J. Clark et al. 2018). We were motivated to search inner-Galaxy sources to try to identify MSPs from the putative bulge population, and so we wish to investigate if PSR J1649–3012 belongs to this population. This requires us to estimate the distance to the pulsar, to determine if it might reside in the Galactic bulge, at a distance of 6–10 kpc from the Solar System, or from the local Galactic disk population closer to Earth.

The gamma-ray source in which we discovered this pulsar was long considered a strong MSP candidate, and as such has been targeted by previous radio surveys¹⁸ of unidentified *Fermi*-LAT sources with the Green Bank

Telescope (GBT) (S. Sanpa-Arsa 2016), and Murriyang (M. Kerr et al. 2025). We folded these archival observations, as well as a dedicated coherent beam formed on our best-fitting timing position during the MMGPS UHF observation, but did not detect any pulsations. This makes PSR J1649–3012 only the third known “radio-quiet” gamma-ray MSP (C. J. Clark et al. 2018; L. Nieder et al. 2020b) that has been subjected to sensitive radio searches without detection. The expected dispersion smearing and scattering timescales for the most sensitive GBT observations are smaller than 10% of the rotation period for all DMs up to the maximum expected DM (248 pc cm⁻³ from NE2001) for this line-of-sight, and so this non-detection is unlikely to be due to dispersive smearing or scattering. The lack of radio detection could be explained by either the pulsar having a low intrinsic radio luminosity, or a radio beam that misses our line-of-sight.

The observed spin-down rate, \dot{f}_{obs} for this pulsar results in an estimated spin-down luminosity, $\dot{E} \approx 1.3 \times 10^{34} \text{ ergs}^{-1}$. However, we must correct the observed spin-down rate for relative acceleration between the pulsar and the SSB. One source of apparent acceleration is the so-called Shklovskii effect (I. S. Shklovskii 1970), whereby initially tangential proper motion picks up an increasingly radial component. The magnitude of this acceleration is distance-dependent, $\Delta\dot{f}_{\text{Shk}} = f\mu^2 d/c$, where $\mu = \sqrt{\mu_\delta^2 + \mu_\alpha^2 \cos^2 \delta}$ is the total proper angular speed. From our gamma-ray timing solution, we obtain a marginal (2.5 σ) detection of proper motion in the R.A. direction ($\mu_\alpha \cos \delta = -5 \pm 2 \text{ mas yr}^{-1}$), but motion in the Decl. direction is less precisely estimated ($\mu_\delta = 7 \pm 11 \text{ mas yr}^{-1}$). As a result, the Shklovskii contribution to the observed spin-down rate is rather uncertain: this effect could be almost negligible, or it could account for all of the observed spin-down at distances greater than around 4 kpc. Relative acceleration due to the Galactic potential, which we evaluate using the PJM17_best.Tpot model of GalPot (P. J. McMillan 2017), is a smaller effect at small distances, but at distances > 7 kpc its contribution to the observed spin-down rate becomes more significant and positive, and therefore allows for larger intrinsic spin-down luminosities. We show the distance-dependence of the inferred intrinsic spin-down luminosity and gamma-ray efficiency in Figure 3. We find that the $\eta \approx 1$ level is possible for all distances $d \gtrsim 2.5$ kpc, even including $d \gtrsim 8$ kpc if the total proper motion is on the lower end of our constraints. However, the range of MSP efficiencies seen in 3PC of 0.01–1 suggests a distance of 1 kpc $\lesssim d \lesssim 6$ kpc is more likely here.

¹⁸ A gamma-ray source, J1649–3004, near this position was also targeted with the Giant Metrewave Radio Telescope (GMRT)

by B. Bhattacharyya et al. (2021), however the timing position of the new pulsar is outside the primary beam of this observation.

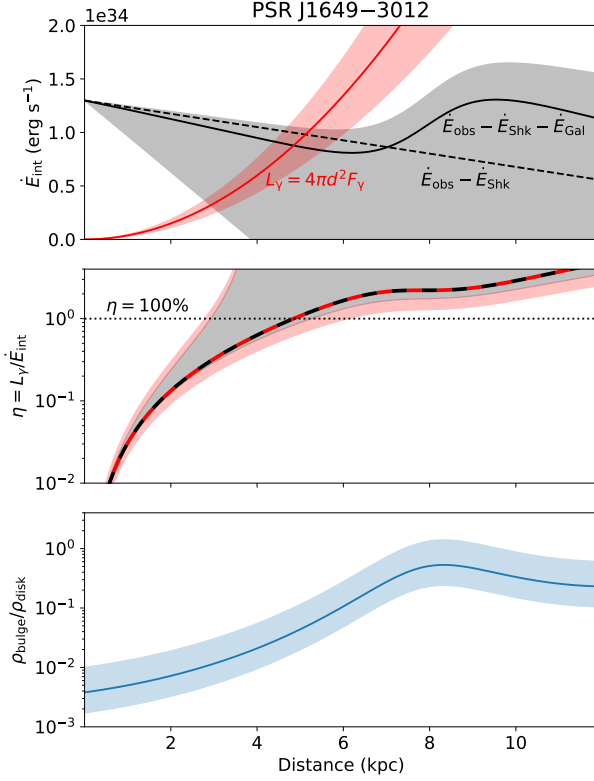


Figure 3. Distance dependence of inferred properties of PSR J1649–3012. The top panel shows the intrinsic spin-down luminosity (\dot{E}_{int}), after correcting for the Shklovskii effect according to our best-fitting timing model (dashed black line) and also the acceleration in the Galactic potential (solid black line). The grey shaded region shows $1-\sigma$ uncertainties on the intrinsic spin-down luminosity, propagated from the uncertainty on the total proper motion, which we assume to be much larger than the uncertainty in the Galactic acceleration. The gamma-ray luminosity (L_γ) and $1-\sigma$ uncertainties according to the observed energy flux (G_γ) from 4FGL-DR4 are shown by the red line and shaded region. The middle panel shows the corresponding gamma-ray efficiency, with the ratio of the red and black lines from the top panel shown by the dashed red and black line. The relative contributions to the efficiency uncertainty from the proper motion and observed flux uncertainties are shown by grey and red shaded regions, respectively. The dotted black line shows a loose upper limit corresponding to 100% efficiency. The bottom panel shows the ratio between the predicted density of MSPs in the putative Galactic bulge population from the model of F. Calore et al. (2016) and in the Galactic disk according to the model of L. Levin et al. (2013).

3.5.2. PSR J1736–3422

With a characteristic age of 84 kyr, this is the youngest pulsar discovered in this work. Due to the double-peaked shape of its pulse profile, *Einstein@Home* only detected the second harmonic as a significant candidate,

but our automatic folding at half the original spin frequency revealed significant excess Fourier power in odd-numbered harmonics, clarifying the fundamental spin frequency as $f \approx 2.88$ Hz.

This pulsar exhibits significant timing noise, illustrated in Figure 4, that contains detectable features even at relatively high frequencies (of a few per year). We were unable to obtain an acceptable model to the observed timing noise power spectrum (shown in Figure 4) using a single cut-off power-law spectrum. This either returned a steep spectrum (with spectral index of $\gamma > 6$) that left excess power at intermediate frequencies of $0.5\text{--}2$ yr $^{-1}$ (and visible residual trends in the resulting photon phases), or a shallow spectrum (with $\gamma \approx 3.5$) that accounted for both high- and low-frequency power, but over-estimated the power at all intermediate frequencies. We therefore added a second smoothly broken power-law component to our model. This two-component model resulted in a more typical steep component at low frequencies (with $\gamma > 6$ at 95% confidence), and a low-amplitude flat component with corner frequency $f_c = 2.0 \pm 0.6$ yr $^{-1}$. The corner frequency of the steep component is constrained only to be similar or below one cycle in the 16 yr observation time, meaning that this component is well modeled by a pure power-law. The spectral index of the high-frequency component is not constrained by the data, since this component falls quickly below the white noise level at frequencies above the corner frequency, so we fixed this parameter at $\gamma_2 = 6$.

This two-component timing noise spectrum is, to our knowledge, highly unusual for a gamma-ray pulsar. Correlated phase and pulse-profile variations have been detected in many radio pulsars (A. Lyne et al. 2010; P. R. Brook et al. 2016; M. E. Lower et al. 2025), including in the gamma-ray pulsars J0742–2822 and J1830–1059 that have similar spin-down luminosities to PSR J1736–3422, which A. Lyne et al. (2010) found could be explained by quasi-periodic switching between two different magnetospheric states, each with a distinct spin-down rate and radio pulse profile shape. By simulating timing noise processes according to that model, we found that we could produce power spectra that were qualitatively similar to the spectrum we measure from J1736–3422, if the switching timescale is around 100 d and varies by around 25%, and the spin-down rate differs by around 2×10^{-15} Hz s $^{-1}$ between the high- and low- states. These values are comparable to those in the A. Lyne et al. (2010) sample, making this a plausible explanation for the observed high-frequency timing noise structure.

However, this hypothesis is difficult to test further. In the absence of detectable radio pulsations, we cannot test for correlated changes in the radio pulse profile, of the kind seen in A. Lyne et al. (2010). The possible switching timescale is also too short for us to sensitively check for similar shape variations in the gamma-

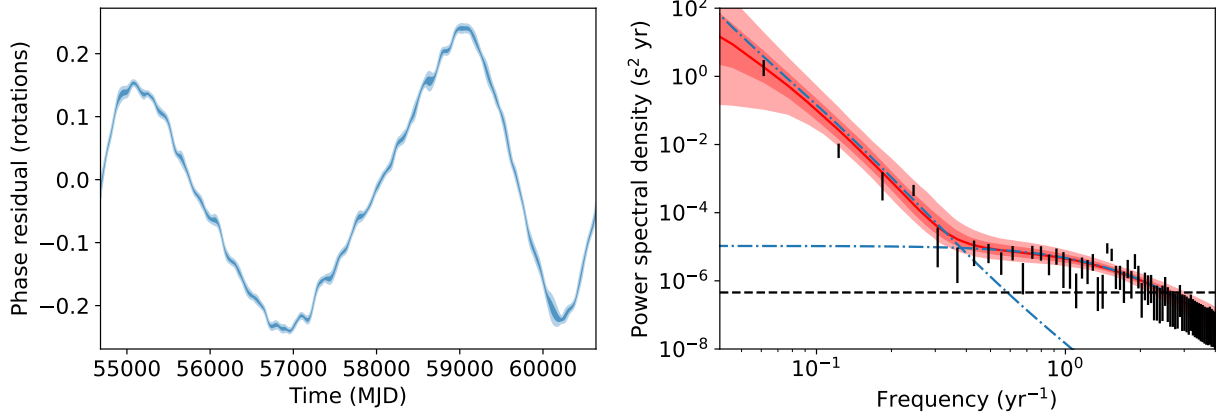


Figure 4. Illustration of timing noise in PSR J1736–3422. The left panel shows the estimated variations in the rotational phase, after subtracting a cubic spin-down model, with the 2σ confidence interval indicated by the blue shaded region. The right panel shows the resulting power spectrum of these phase variations. The black error bars show the 1σ posterior uncertainties on the Fourier powers, marginalised over the underlying timing model and template pulse profile shape. The blue dot-dashed lines show the best fitting models for the two noise components, while the red line and shaded region shows the best-fitting model and uncertainty regions for the full noise model prior. The estimated white-noise level is shown by the black dashed line. The posterior distributions for high frequencies are all below this level, and closely follow the priors as a result.

ray pulse profile. Despite several of the magnetospheric-switching radio pulsars also being detected in gamma rays, flux and pulse-profile variability has only been detected from one gamma-ray pulsar, PSR 2021+4026 (A. Allafort et al. 2013; H. H. Wang et al. 2024). That pulsar does appear to transition between long-lived gamma-ray flux/spin-down states, but the spin-down variations are orders of magnitude larger than we observe here, suggesting much larger global changes in the magnetosphere are at play there (A. Fiori et al. 2024).

PSR J1736–3422 is one of only two young (< 100 kyr) pulsars within one degree of the supernova remnant (SNR) G354.8–0.8, with C. M. Espinoza et al. (2022) concluding that the younger and more nearby PSR J1734–3333 (21' from the SNR) cannot be associated with this remnant. The age and distance to this SNR are unclear, but we can use the characteristic age and estimated distance for PSR J1736–3422 to investigate a possible association. The angular separation of 40' between this pulsar and the SNR would require a proper motion of around 30 mas yr^{-1} , which would not be detectable to our gamma-ray timing analysis¹⁹. From the gamma-ray flux reported in 4FGL-DR4, and using the heuristic efficiency, we find that the distance to PSR J1736–3422 is likely to be between 1 and 4 kpc. The required proper motion therefore corresponds to a plausible kick velocity of $(d/1 \text{ kpc}) \times 140 \text{ km s}^{-1}$. There is no sign of any radio emission in the SMGPS image covering this pulsar (see Figure 2), either as a point source or from a bow-shock that would provide evidence that

the pulsar is traveling with high velocity through the interstellar medium. The association between this pulsar and the SNR therefore remains plausible, but speculative.

3.5.3. PSR J1742–3321

This is a middle-aged (2 Myr) pulsar found in a *Fermi*-LAT source lying 4.5° from the GC. Based on the estimated spin-down power of $1.7 \times 10^{34} \text{ erg s}^{-1}$, we estimate the distance to lie in the range of $0.8 \text{ kpc} < d < 3 \text{ kpc}$.

This pulsar also exhibits deviations from a linear spin-down model, but in this case we were able to model this as a small glitch occurring in 2016 January, with a fractional frequency increment $\Delta f_g/f \approx 2 \times 10^{-9}$. This glitch size is very typical of the low-magnitude glitches in the bi-modal glitch distribution found by A. Basu et al. (2022). While this glitch happened within the span of our search data set, it had very little impact on our search sensitivity; the magnitude is small enough that the pulsed signal still remains well in phase over the coherence time of our semi-coherent search (during which time a phase shift of only $\Delta\phi = \Delta f_g T = 0.062$ rotations would accumulate).

3.5.4. PSR J1748–2815

At an angular separation of 0.93° , this has the smallest known angular separation of any gamma-ray pulsar to the GC, and was found in the closest source to the GC in our target list. The next closest gamma-ray pulsar, PSR J1747–2958, (1.09° from the GC) was originally found in a radio search of the “Mouse” nebula (F. Camilo et al. 2002).

This location poses a particular challenge for gamma-ray spectral and spatial modelling: this pulsar and the

¹⁹ The detection of the much smaller proper motion from the MSP J1649–3012 was possible because the uncertainty on astrometric parameters scales inversely with the pulsar’s spin frequency.

GC are separated by less than the 68% containment angle of the LAT point spread function²⁰ for all photon energies below 800 MeV. Flux from this pulsar therefore represents a contaminating factor for measuring the spectral and spatial properties of the GC excess at low energies, and vice versa. Additionally, this position within the Galactic plane has an unusually high contribution from the diffuse interstellar emission; this pulsar lies adjacent to the two brightest pixels in the `g11_iem_v07.fits` interstellar emission model used to construct the [S. Abdollahi et al. \(2020\)](#) catalog and its incremental releases. As a result of this, the estimated significance and spectrum of the gamma-ray flux from this pulsar depends strongly on the chosen background model and analysis methods. Despite appearing as a highly significant source in the earlier *Fermi*-LAT Third Source Catalog ([F. Acero et al. 2015](#)) and in the **2FIG** catalog used here, this pulsar was not even identified as a significant point source in **4FGL-DR4**. This is likely due to a combination of flux from this source being misattributed to the diffuse background model or to other nearby sources, and the weighted log-likelihood method used in **4FGL** to downweight the significance of residual flux in regions of the sky where systematic uncertainties in the background model dominate over statistical uncertainties.

Our discovery of gamma-ray pulsations from this source therefore provides a valuable “anchor” for gamma-ray modelling of the GC region, as we can use the pulsed nature of the emission from this source to more confidently disentangle this source from its surroundings. We do this in a multi-step process: first, we applied the “simple weighting” scheme of [P. Bruel \(2019\)](#) to compute approximate photon weights without requiring an accurate gamma-ray sky model, using a reference energy of $10^{4.2}$ MeV ≈ 16 GeV that maximized the weighted H -test. Next, we used these initial weights to obtain a preliminary timing solution, which we could then use to apply the “model weighting” scheme from [P. Bruel \(2019\)](#), in which the parameters of an exponentially-cutoff power-law spectrum model for the pulsar are varied to maximise the resulting weighted H -test. These updated weights were then used to perform the full timing analysis, including a red timing noise model, as described in Section 3.1. Finally, using this resulting timing solution, we computed the phase of SOURCE-class photons, according to the `P8R3_SOURCE_V3` IRFs, detected up to MJD 60524 (2024 August 02), with energies $63 \text{ MeV} < E < 31.6 \text{ GeV}$, and with zenith angles $< 105^\circ$. We separated these into on- and off-pulse phase ranges by employing the Bayesian Blocks algorithm ([J. D. Scargle 1998](#)) on the weighted pulse profile, and binned these in energy and angular direc-

tion to obtain energy-dependent on- and off-pulse counts maps. The on/off-pulse phase intervals determined by the Bayesian Blocks method depend on the prescription used for computing the uncertainty on the weighted photon counts in each phase bin, and is either 0.26–0.65 (for Poisson uncertainties, $\sqrt{\sum_j w_j^2}$) or 0.34–0.65 (for uncertainties of $\sqrt{1 + \sum_j w_j^2}$, as used in e.g. [A. A. Abdo et al. 2013](#)).

Assuming there is no un-pulsed emission from this pulsar, which is the case for most known gamma-ray pulsars (**3PC**), the on-pulse map selection should contain all of the flux from the pulsar, while it should be entirely absent from the off-pulse map. Subtracting the off-pulse counts from the on-pulse counts (weighted by the relative phase ranges covered by the on- and off-pulse phase selections) should therefore result in a difference image where the background is consistent with zero (within the uncertainties), and remaining excess flux is entirely attributable to the pulsar. We can therefore fit the spectrum of the excess counts to estimate the spectrum of the pulsar, without needing to model the flux of any other source, including the GC, and the diffuse interstellar emission. The on- and off-pulse counts maps and difference images for different energy bands are shown in Figure 5. The Mouse pulsar, J1747–2958, is also visible as a point source in these counts maps. Its spectrum could be similarly estimated from the on- and off-pulse counts to aid investigations the Galactic Center flux, although its larger separation from the Galactic plane ($|b| = 0.84^\circ$) makes this less crucial.

We modeled the pulsar spectrum as a sub-exponentially-cutoff power law, $dN/dE \propto (E/1000 \text{ MeV})^{-\Gamma} \exp(-aE^{2/3})$ and used the Fermi tools to compute the expected count map from a point source at the pulsar position. Fitting the count spectrum within the PSF 68% containment radius gives a spectral index $\Gamma = 1.07 \pm 0.16 \pm 0.09$, exponential factor $a = (6.0 \pm 1.0 \pm 0.03) \times 10^{-3}$, and an integrated energy flux above 100 MeV of $(2.8 \pm 0.2 \pm 0.4) \times 10^{-11} \text{ erg cm}^{-2} \text{ s}^{-1}$, where the first (statistical) uncertainties are obtained using the wider on-pulse phase definition (0.26–0.65), and the second (systematic) uncertainties show the shift from changing to the narrower (0.34–0.65) on-pulse region. This flux is only around 60% of the value for this source in [F. Acero et al. \(2015\)](#), suggesting that the previous catalog analyses significantly over-estimated the flux from this source.

Comparing this energy flux to the pulsar’s spin-down luminosity, $E = 1.4 \times 10^{35} \text{ erg s}^{-1}$, we find a 100%-efficiency distance upper limit of around 7 kpc, but a heuristic luminosity distance of $1 \text{ kpc} < d < 4 \text{ kpc}$. It is therefore most likely that this is also a foreground pulsar, rather than one that originated from a GC pulsar population.

²⁰ https://www.slac.stanford.edu/exp/glast/groups/canda/lat_Performance.htm

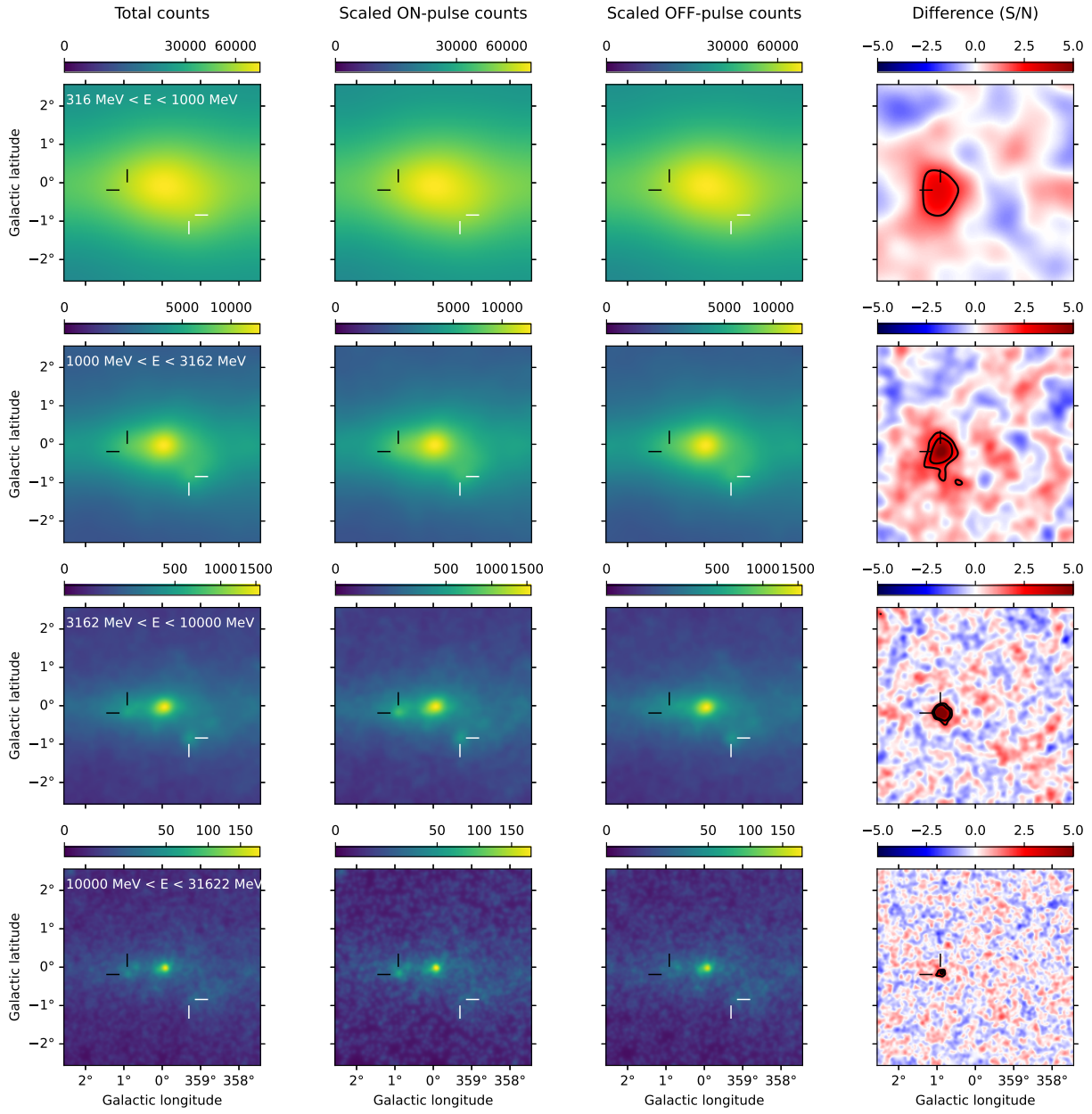


Figure 5. Gamma-ray photon counts maps of the Galactic Center region. Each row shows counts maps for logarithmically-spaced energy bands, convolved with the *Fermi*-LAT point-spread function for the highest energy in that band. The gamma-ray timing position of PSR J1748–2815 is highlighted by black markers. In each row panels show, from left to right: the total photon counts, on-pulse photon counts (divided by the on-pulse phase fraction to maintain the same color scale as the total count maps), off-pulse photon counts (divided by the off-pulse phase fraction), and the difference between the rescaled on- and off-pulse maps in signal-to-noise units. Counts maps have a square-root scaling, indicated on the color bars. Contour lines on the difference images are at the 2σ and 3σ level. The point source visible at $(l, b) = (359.3^\circ, -0.8^\circ)$, highlighted by white markers, is another gamma-ray pulsar, PSR J1747–2958.

The timing noise model for this pulsar has a lower amplitude than that of PSR J1736–3422, and is consistent with a simple power-law form with $\gamma > 2.5$. These properties are broadly consistent with those of similarly energetic gamma-ray pulsars timed by [M. Kerr et al. \(2015\)](#).

We found archival radio observations from Murriyang covering the location of PSR J1748–2815 as part of the Breakthrough Listen project ([V. Gajjar et al. 2021](#); [V. Gajjar et al. 2020](#)), using the Ultra-Wide-bandwidth Low-frequency (UWL) receiver ([G. Hobbs et al. 2020](#)). These consisted of observations on two epochs in which this position was covered three times with 10-minute pointings separated by 10-minute observations of another nearby field. We found no significant radio pulsations in any individual 10-minute observation, or in the stacked data. While our gamma-ray ephemeris is sufficient for stacking observations taken on the same epoch, the uncertainty on our timing solution is large enough that there may be a small relative phase offset between the two observations, greater than the phase binning of our radio fold, meaning that we cannot guarantee that a putative radio pulse would lie within the same phase bin in both observations. We therefore report upper limits on the radio flux density from single epochs, rather than the upper limit from stacking all of the Murriyang data, although this also resulted in a non-detection.

The MeerKAT Galactic Center Mosaic ([I. Heywood et al. 2022](#)), shown in Figure 2, shows that PSR J1748–2815 lies close to the SNR G1.0–0.1, near the end of a tail-like structure protruding from the SNR, and also near the end of a likely non-thermal radio filament, although the gamma-ray timing position is significantly offset from all of these. Given the high density of radio-emitting sources in the busy GC region, and that our heuristic distance estimate places this pulsar well in front of the GC, it seems unlikely that the pulsar is associated with any of these structures.

4. DISCUSSION

We were motivated to perform our survey for new gamma-ray pulsars in the inner Galaxy to identify bright, isolated MSPs that from a putative bulge population that could explain the observed Galactic center gamma-ray excess.

We found in Section 3.5 that all of the new pulsars are likely to lie significantly closer to Earth than to the GC, making it likely that they all belong to the standard Galactic disk population. However, for the one new MSP that we discovered, PSR J1649–3012, there was a chance that it could lie at larger distances from Earth, up to around 8 kpc, that could make an origin in the Galactic bulge possible. To evaluate the chance of this MSP being from the putative bulge population, we compared the predicted MSP densities along the line-of-sight to PSR J1649–3012 from models of the Galactic thick-disk and bulge MSP populations. For the for-

mer, we took the model from [L. Levin et al. \(2013\)](#), which has a total of 83000 ± 42000 MSPs with a Gaussian distribution with width 4.5 kpc in cylindrical radius around the Galactic center and an exponential distribution in the height above the Galactic plane with scale height 0.5 kpc. For the bulge population, we took the model from [F. Calore et al. \(2016\)](#), which has a total of 9200 ± 3100 MSPs within a radius of 3 kpc around the center of the Galaxy (similar to our $40^\circ \times 40^\circ$ search region), in a spherically symmetrical distribution with density falling off with galactocentric distance as $r^{-2.56}$. The ratio of these two densities $\rho_{\text{bulge}}/\rho_{\text{disk}}$ is shown in Figure 3. The disk model predicts a larger MSP density than the bulge model at all distances, by more than an order-of-magnitude for distances below 6 kpc, but this ratio could be close to unity at distances of around 8 kpc. Hence it is not impossible that this MSP originated in the Galactic bulge, but given that a wide range of more typical efficiencies result in distances for which the disk model is strongly favored, we conclude that it is more likely that this pulsar belongs to the normal Galactic disk population.

However, while we find that it is unlikely that we have found any new pulsars belonging to a putative bulge population, we emphasize that our results in no way rule out the presence of such a population.

Due to the necessary compromise between computing cost and sensitivity, our semi-coherent search method is only able to detect gamma-ray pulsations from fairly bright sources, and could therefore only identify new GC MSPs in the upper tail of the luminosity distribution. To estimate how much less sensitive our searches are compared to a fully-coherent search for pulsations from a known pulsar where the ephemeris parameters are already measured from a radio timing campaign, we consider the relevant test statistics, S and \mathcal{P} . As derived in [L. Nieder et al. \(2020a\)](#), both test statistics have spectral signal-to-noise ratios θ_S^2 and $\theta_{\mathcal{P}}^2$ proportional to the sum of the squared photon weights ($W^2 = \sum_j w_j^2$), with θ_S^2 being lower by a factor of $\sqrt{T/T_{\text{obs}}}$. We show in Appendix B that W^2 is proportional to the square of the pulsar photon flux.

These test statistics have different noise distributions (normal and chi-squared, respectively) and the two search methods have different associated trials factors, meaning we must consider different significance thresholds for each. [D. A. Smith et al. \(2019\)](#) showed that a threshold of $H = 25$ is a sufficiently conservative threshold for detecting gamma-ray pulsations when folding with a radio ephemeris. Since most gamma-ray pulse profiles have most power in the fundamental harmonic, we consider a threshold of $\mathcal{P} \approx 20$, corresponding to $\theta_{\mathcal{P}}^2 = 9$. For our semi-coherent searches, we find an empirical threshold of $\theta_S^2 = 8$ for candidate signals entering the follow-up stages of our hierarchical search.

We can therefore estimate the relative flux thresholds of our semi-coherent search compared to searches for gamma-ray pulsations from radio pulsars with well-known ephemerides as:

$$\begin{aligned} \frac{F_S^*}{F_P^*} &= \left(\frac{\theta_S^2}{\theta_P^2} \right)^{1/2} \left(\frac{T_{\text{obs}}}{T} \right)^{1/4}, \\ &= \left(\frac{8}{9} \right)^{1/2} \left(\frac{16 \text{ yr}}{2^{22} \text{ s}} \right), \\ &\approx 3.1. \end{aligned} \quad (9)$$

D. A. Smith et al. (2019) demonstrated that gamma-ray pulsations can be detected from sources all the way down to, and sometimes even below, the 4FGL point-source threshold. Hence, the coherent Fourier power has a similar photon flux threshold as the *Fermi*-LAT point-source significance threshold. We are therefore only sensitive to sources that have photon fluxes that are around 3.1 times larger than the 4FGL detection threshold to be detectable in our searches.

Recent analyses of the GC excess have found that, under the MSP population explanation, only $\mathcal{O}(20)$ MSPs should be individually detectable as gamma-ray point sources in the latest *Fermi*-LAT data (e.g. I. Holst & D. Hooper 2024; D. V. Malyshev 2024). The relatively higher threshold of our semi-coherent search means that only around 50% of these are bright enough to be detectable in our searches, leaving only around $\mathcal{O}(10)$ detectable pulsars. More importantly, around 80% of Galactic MSPs are in binary systems, and therefore undetectable to our searches, and this fraction may even be under-estimated due to historic biases against detecting short-period binary MSPs (P. Bangale et al. 2024).

The number of GC MSPs that we might have expected to detect in a perfect survey for isolated pulsars in inner-Galaxy sources is therefore likely to be only around one or two. The fact that we did not detect any MSPs that can be attributed to this population is therefore not surprising, nor at odds with the MSP explanation for the GC excess.

The lack of sensitivity of our searches to binary MSPs may indeed be one of the largest barriers to detecting the GC MSP population through gamma-ray pulsation searches. The new pulsation searching method of D. Gazith et al. (2024) does not have this shortcoming, although it remains unclear how well that method will cope in the inner Galaxy, where the high background level means that pulsar signals tend to consist of a large number of relatively low-weight photons, rather than a smaller number of high-weight photons.

The lack of candidate GC MSPs in 3PC has been interpreted as evidence against the GC population (I. Holst & D. Hooper 2024). However, the detection of a pulsar as a gamma-ray point source was not a sufficient (nor even necessary) criterion for inclusion in 3PC, where the only requirement was the significant detection

of gamma-ray pulsations. For faint sources, such a detection requires a radio timing solution that either covers or can be extrapolated back to the start of the *Fermi* mission. Radio pulsar searches of the inner Galaxy are, however, particularly challenging, due to the large distance and high background of radio-emitting sources that reduce sensitivity, and the high level of scattering and dispersion from the interstellar medium that smear out pulses and particularly affect searches for rapidly spinning MSPs. These propagation effects are particularly strong at low radio frequencies $\lesssim \mathcal{O}(1 \text{ GHz})$, where most large-scale pulsar surveys have historically taken place, and where pulsars tend to be brightest due to their steep power-law spectra (A. Karastergiou et al. 2024). The particular challenge of detecting MSPs in the inner Galaxy is highlighted by the fact that the only known MSP within 1° of the GC was only recently discovered (M. E. Lower et al. 2024), and was only detectable at $\gtrsim 2 \text{ GHz}$, requiring the novel wide-band high-frequency coverage of the UWL receiver on Murriyang (G. Hobbs et al. 2020).

Recent analyses have found that some sources in the inner Galaxy are now becoming individually detectable as resolved sources, with spectra consistent with MSPs (D. V. Malyshev 2024), but it may require next-generation radio telescopes, and long radio timing campaigns before these can be identified as gamma-ray pulsars.

Due to the large overlap between the expected bulge and disk populations (evident in the lower panel of Figure 3), evidence for a bulge MSP population that could explain the GC gamma-ray excess will require the detection of a large overdensity of MSPs in the inner Galaxy relative to the rest of the Galactic disk. Efforts are underway to identify candidate pulsars in X-ray (J. Berteaud et al. 2021, 2024) and radio imaging surveys (D. A. Frail et al. 2024), and indeed three new MSPs have recently been discovered by targeting candidate sources identified by these surveys (J. Berteaud, A&A, submitted; S. D. Hyman et al. 2025). These may represent the tip of the iceberg for the bulge population. While we did not find any new MSPs here that are likely to be associated to the bulge population, we have shown that gamma-ray searches could possibly contribute one or two new members to this population. A renewed survey similar to the one performed here, but with a longer data set, new gamma-ray sources, and a longer coherence time to increase sensitivity, may yet contribute to uncovering this population.

5. CONCLUSIONS

We performed searches for gamma-ray pulsations from 55 sources in the inner Galaxy ($-20^\circ < l < 20^\circ$, $-20^\circ < b < 20^\circ$), identifying 4 of these as new gamma-ray pulsars. None of these pulsars have been detected in radio observations, including the isolated MSP

J1649–3012 that is now only the third confirmed “radio-quiet” gamma-ray MSP.

One of these pulsars, J1748–2815, has the smallest angular separation to the GC of any known gamma-ray pulsar, at 0.93° . This pulsar is not detected as a point source in **4FGL-DR4**, likely due to some of its flux being misattributed to the diffuse background in that direction. This suggests that a strategy of searching a large grid of sky locations covering the innermost part of the Galaxy, using the methods of [P. Bruel \(2019\)](#) to weight photons regardless of whether or not a significant source is detected at that position, may be able to reveal additional pulsars. We performed a phase-resolved analysis that allows us to disentangle its flux from the surrounding area, which provides a spectral anchor point for the development of new interstellar gamma-ray emission models.

The estimated distances to these pulsars, based on their measured gamma-ray fluxes and assuming typical spin-down/gamma-ray efficiencies suggest that they are all more likely to be foreground sources than from a putative bulge population that may explain the GC GeV excess, but our results in no way rule out the presence of such a population.

Nevertheless, our discoveries demonstrate our ability to find new pulsars in this region of the sky, and suggest that new searches of the inner Galaxy, with the extra years of LAT data and newly identified gamma-ray sources that have accumulated since we began this project, may soon be able to identify the brightest isolated pulsars from this putative population.

ACKNOWLEDGMENTS

We gratefully acknowledge the contributions of the *Einstein@Home* volunteers, without whom this work would not have been possible. We would particularly like to thank the volunteers whose computers discovered the new pulsars presented in this work,

- PSR J1649–3012: Alexander Kravchenko, Moscow, Russia, and the ATLAS cluster, Hannover, Germany;
- PSR J1736–3422: the ATLAS cluster, Hannover, Germany;
- PSR J1742–3321: Lingnan Cai, Nanjing, China, and the ATLAS cluster, Hannover, Germany;
- PSR J1748–2815: Duncan Brown, Syracuse, NY, USA, and Miguel Angel Gonzalo, Madrid, Spain.

Einstein@Home is supported by National Science Foundation grant NSF 1816904.

Work at NRL is supported by NASA.

We thank Paul S. Ray and Giacomo Principe for reviewing this paper on behalf of the *Fermi*-LAT collaboration. We also thank Bhaswati Bhattacharyya and

Jayanta Roy for investigating archival GMRT observations to check for previous coverage of PSR J1649–3012.

The *Fermi* LAT Collaboration acknowledges generous ongoing support from a number of agencies and institutes that have supported both the development and the operation of the LAT as well as scientific data analysis. These include the National Aeronautics and Space Administration and the Department of Energy in the United States, the Commissariat à l’Energie Atomique and the Centre National de la Recherche Scientifique / Institut National de Physique Nucléaire et de Physique des Particules in France, the Agenzia Spaziale Italiana and the Istituto Nazionale di Fisica Nucleare in Italy, the Ministry of Education, Culture, Sports, Science and Technology (MEXT), High Energy Accelerator Research Organization (KEK) and Japan Aerospace Exploration Agency (JAXA) in Japan, and the K. A. Wallenberg Foundation, the Swedish Research Council and the Swedish National Space Board in Sweden. Additional support for science analysis during the operations phase is gratefully acknowledged from the Istituto Nazionale di Astrofisica in Italy and the Centre National d’Études Spatiales in France. This work performed in part under DOE Contract DE-AC02-76SF00515.

The MeerKAT telescope is operated by the South African Radio Astronomy Observatory, which is a facility of the National Research Foundation, an agency of the Department of Science and Innovation. This work has made use of the “MPIfR S-band receiver system” designed, constructed and maintained by funding of the MPI für Radioastronomie (MPIfR) and the Max-Planck-Society (MPG). Observations used the FBFUSE and APSUSE computing clusters for data acquisition, storage and analysis. These clusters were funded, designed and installed by the MPIfR and the MPG. FBFUSE performs beamforming operations in real-time using the `mosaic`²¹ software stack ([W. Chen et al. 2021](#)). The MPIfR-MeerKAT Galactic Plane Survey is led by the MPIfR and is supported by the MPG.

Murriyang, CSIRO’s Parkes radio telescope, is part of the Australia Telescope National Facility²² which is funded by the Australian Government for operation as a National Facility managed by CSIRO. We acknowledge the Wiradjuri people as the Traditional Owners of the Observatory site.

The Green Bank Observatory is a facility of the National Science Foundation operated under cooperative agreement by Associated Universities, Inc.

This research has made use of data or software obtained from the Gravitational Wave Open Science Center ([gwosc.org](#)), a service of the LIGO Scientific Collaboration, the Virgo Collaboration, and KAGRA. This material is based upon work supported by NSF’s LIGO

²¹ <https://github.com/wchenastro/Mosaic>

²² <https://ror.org/05qajvd42>

Laboratory which is a major facility fully funded by the National Science Foundation, as well as the Science and Technology Facilities Council (STFC) of the United Kingdom, the Max-Planck-Society (MPS), and the State of Niedersachsen/Germany for support of the construction of Advanced LIGO and construction and operation of the GEO600 detector. Additional support for Advanced LIGO was provided by the Australian Research Council. Virgo is funded, through the European Gravitational Observatory (EGO), by the French Centre National de Recherche Scientifique (CNRS), the Italian Istituto Nazionale di Fisica Nucleare (INFN) and the Dutch Nikhef, with contributions by institutions from Belgium, Germany, Greece, Hungary, Ireland, Japan, Monaco, Poland, Portugal, Spain. KAGRA is supported by Ministry of Education, Culture, Sports, Science and Technology (MEXT), Japan Society for the Promotion of Science (JSPS) in Japan; National Research Founda-

tion (NRF) and Ministry of Science and ICT (MSIT) in Korea; Academia Sinica (AS) and National Science and Technology Council (NSTC) in Taiwan.

Facilities: Fermi, GBT, LIGO, MeerKAT, Parkes

Software: Astropy (Astropy Collaboration et al. 2013, 2018, 2022), bilby (G. Ashton et al. 2019), BOINC (D. P. Anderson 2020), dsspr (W. van Straten & M. Bailes 2011), dynesty (J. S. Speagle 2020; S. Koposov et al. 2024), Fermi tools (Fermi Science Support Development Team 2019), fermipy (M. Wood et al. 2017), FFTW (M. Frigo & S. G. Johnson 2005), GalPot (P. J. McMillan 2017), LALSuite (LIGO Scientific Collaboration 2020), matplotlib (J. D. Hunter 2007), numpy (C. R. Harris et al. 2020), psrchive (W. van Straten et al. 2011), PulsarX (Y. Men et al. 2023), PINT (J. Luo et al. 2018)

REFERENCES

Abazajian, K. N. 2011, *JCAP*, 2011, 010, doi: [10.1088/1475-7516/2011/03/010](https://doi.org/10.1088/1475-7516/2011/03/010)

Abazajian, K. N., & Kaplinghat, M. 2012, *PhRvD*, 86, 083511, doi: [10.1103/PhysRevD.86.083511](https://doi.org/10.1103/PhysRevD.86.083511)

Abbott, B. P., Abbott, R., Abbott, T. D., et al. 2019, *The Astrophysical Journal*, 879, 10, doi: [10.3847/1538-4357/ab20cb](https://doi.org/10.3847/1538-4357/ab20cb)

Abbott, R., et al. 2021, *SoftwareX*, 13, 100658, doi: [10.1016/j.softx.2021.100658](https://doi.org/10.1016/j.softx.2021.100658)

Abbott, R., Abbott, T. D., Acernese, F., et al. 2022, *ApJ*, 932, 133, doi: [10.3847/1538-4357/ac6ad0](https://doi.org/10.3847/1538-4357/ac6ad0)

Abbott, R., et al. 2023, *Astrophys. J. Suppl.*, 267, 29, doi: [10.3847/1538-4365/acdc9f](https://doi.org/10.3847/1538-4365/acdc9f)

Abdo, A. A., Ackermann, M., Ajello, M., et al. 2009, *Science*, 325, 840, doi: [10.1126/science.1175558](https://doi.org/10.1126/science.1175558)

Abdo, A. A., Ajello, M., Allafort, A., et al. 2013, *ApJS*, 208, 17, doi: [10.1088/0067-0049/208/2/17](https://doi.org/10.1088/0067-0049/208/2/17)

Abdollahi, S., Acero, F., Ackermann, M., et al. 2020, *ApJS*, 247, 33, doi: [10.3847/1538-4365/ab6bcb](https://doi.org/10.3847/1538-4365/ab6bcb)

Acero, F., Ackermann, M., Ajello, M., et al. 2015, *ApJS*, 218, 23, doi: [10.1088/0067-0049/218/2/23](https://doi.org/10.1088/0067-0049/218/2/23)

Ackermann, M., Ajello, M., Albert, A., et al. 2011, *PhRvL*, 107, 241302, doi: [10.1103/PhysRevLett.107.241302](https://doi.org/10.1103/PhysRevLett.107.241302)

Ackermann, M., Ajello, M., Albert, A., et al. 2017, *ApJ*, 840, 43, doi: [10.3847/1538-4357/aa6cab](https://doi.org/10.3847/1538-4357/aa6cab)

Allafort, A., Baldini, L., Ballet, J., et al. 2013, *ApJL*, 777, L2, doi: [10.1088/2041-8205/777/1/L2](https://doi.org/10.1088/2041-8205/777/1/L2)

Allen, B. 2021, *PhRvD*, 104, 042005, doi: [10.1103/PhysRevD.104.042005](https://doi.org/10.1103/PhysRevD.104.042005)

Allen, B., Knispel, B., Cordes, J. M., et al. 2013, *ApJ*, 773, 91, doi: [10.1088/0004-637X/773/2/91](https://doi.org/10.1088/0004-637X/773/2/91)

Anderson, D. P. 2020, *Journal of Grid Computing*, 18, 99, doi: [10.1007/s10723-019-09497-9](https://doi.org/10.1007/s10723-019-09497-9)

Arons, J. 1996, *A&AS*, 120, 49

Ashok, A. 2023, PhD thesis, Leibniz Universität Hannover, doi: [10.15488/14733](https://doi.org/10.15488/14733)

Ashok, A., Covas, P. B., Prix, R., & Papa, M. A. 2024, *PhRvD*, 109, 104002, doi: [10.1103/PhysRevD.109.104002](https://doi.org/10.1103/PhysRevD.109.104002)

Ashok, A., Beheshtipour, B., Papa, M. A., et al. 2021, *The Astrophysical Journal*, 923, 85, doi: [10.3847/1538-4357/ac2582](https://doi.org/10.3847/1538-4357/ac2582)

Ashton, G., Hübner, M., Lasky, P. D., et al. 2019, *ApJS*, 241, 27, doi: [10.3847/1538-4365/ab06fc](https://doi.org/10.3847/1538-4365/ab06fc)

Astropy Collaboration, Robitaille, T. P., Tollerud, E. J., et al. 2013, *A&A*, 558, A33, doi: [10.1051/0004-6361/201322068](https://doi.org/10.1051/0004-6361/201322068)

Astropy Collaboration, Price-Whelan, A. M., Sipőcz, B. M., et al. 2018, *AJ*, 156, 123, doi: [10.3847/1538-3881/aabc4f](https://doi.org/10.3847/1538-3881/aabc4f)

Astropy Collaboration, Price-Whelan, A. M., Lim, P. L., et al. 2022, *ApJ*, 935, 167, doi: [10.3847/1538-4357/ac7c74](https://doi.org/10.3847/1538-4357/ac7c74)

Atwood, W., Albert, A., Baldini, L., et al. 2013, in *Proceedings of the 4th Fermi Symposium*, Monterey, California, 2012, ed. T. J. Brandt, N. Omodei, & C. Wilson-Hodge, eConf C121028, 8

Atwood, W. B., Ziegler, M., Johnson, R. P., & Baughman, B. M. 2006, *ApJL*, 652, L49, doi: [10.1086/510018](https://doi.org/10.1086/510018)

Atwood, W. B., Abdo, A. A., Ackermann, M., et al. 2009, *ApJ*, 697, 1071, doi: [10.1088/0004-637X/697/2/1071](https://doi.org/10.1088/0004-637X/697/2/1071)

Aulbert, C., & Fehrmann, H. 2008, *Forschungsbericht 2008 - Max-Planck-Institut für Gravitationsphysik, Teilinstitut Hannover*, <https://www.mpg.de/308429/forschungsSchwerpunkt>

Balasubramanian, R., Sathyaprakash, B. S., & Dhurandhar, S. V. 1996, *PhRvD*, 53, 3033, doi: [10.1103/PhysRevD.53.3033](https://doi.org/10.1103/PhysRevD.53.3033)

Ballet, J., Bruel, P., Burnett, T. H., Lott, B., & The Fermi-LAT collaboration. 2023, arXiv e-prints, arXiv:2307.12546, doi: [10.48550/arXiv.2307.12546](https://doi.org/10.48550/arXiv.2307.12546)

Bangale, P., Bhattacharyya, B., Camilo, F., et al. 2024, *ApJ*, 966, 161, doi: [10.3847/1538-4357/ad2994](https://doi.org/10.3847/1538-4357/ad2994)

Barr, E. D., Guillemot, L., Champion, D. J., et al. 2013, *MNRAS*, 429, 1633, doi: [10.1093/mnras/sts449](https://doi.org/10.1093/mnras/sts449)

Basu, A., Shaw, B., Antonopoulou, D., et al. 2022, *MNRAS*, 510, 4049, doi: [10.1093/mnras/stab3336](https://doi.org/10.1093/mnras/stab3336)

Berteaud, J., Calore, F., Clavel, M., et al. 2024, *A&A*, 690, A330, doi: [10.1051/0004-6361/202449473](https://doi.org/10.1051/0004-6361/202449473)

Berteaud, J., Calore, F., Clavel, M., et al. 2021, *PhRvD*, 104, 043007, doi: [10.1103/PhysRevD.104.043007](https://doi.org/10.1103/PhysRevD.104.043007)

Bhattacharyya, B., Roy, J., Johnson, T. J., et al. 2021, *ApJ*, 910, 160, doi: [10.3847/1538-4357/abe4d5](https://doi.org/10.3847/1538-4357/abe4d5)

Bickel, P., Kleijn, B., & Rice, J. 2008, *ApJ*, 685, 384, doi: [10.1086/590399](https://doi.org/10.1086/590399)

Brady, P. R., Creighton, T., Cutler, C., & Schutz, B. F. 1998, *PhRvD*, 57, 2101, doi: [10.1103/PhysRevD.57.2101](https://doi.org/10.1103/PhysRevD.57.2101)

Brook, P. R., Karastergiou, A., Johnston, S., et al. 2016, *MNRAS*, 456, 1374, doi: [10.1093/mnras/stv2715](https://doi.org/10.1093/mnras/stv2715)

Bruel, P. 2019, *A&A*, 622, A108, doi: [10.1051/0004-6361/201834555](https://doi.org/10.1051/0004-6361/201834555)

Bruel, P., Burnett, T. H., Digel, S. W., et al. 2018, arXiv e-prints, arXiv:1810.11394. <https://arxiv.org/abs/1810.11394>

Calore, F., Cholis, I., & Weniger, C. 2015, *JCAP*, 2015, 038, doi: [10.1088/1475-7516/2015/03/038](https://doi.org/10.1088/1475-7516/2015/03/038)

Calore, F., Di Mauro, M., Donato, F., Hessels, J. W. T., & Weniger, C. 2016, *ApJ*, 827, 143, doi: [10.3847/0004-637X/827/2/143](https://doi.org/10.3847/0004-637X/827/2/143)

Camilo, F., Manchester, R. N., Gaensler, B. M., & Lorimer, D. R. 2002, *ApJL*, 579, L25, doi: [10.1086/344832](https://doi.org/10.1086/344832)

Chen, W., Barr, E., Karuppusamy, R., Kramer, M., & Stappers, B. 2021, *Journal of Astronomical Instrumentation*, 10, 2150013, doi: [10.1142/S2251171721500136](https://doi.org/10.1142/S2251171721500136)

Clark, C. J., Pletsch, H. J., Wu, J., et al. 2015, *ApJL*, 809, L2, doi: [10.1088/2041-8205/809/1/L2](https://doi.org/10.1088/2041-8205/809/1/L2)

Clark, C. J., Wu, J., Pletsch, H. J., et al. 2017, *ApJ*, 834, 106, doi: [10.3847/1538-4357/834/2/106](https://doi.org/10.3847/1538-4357/834/2/106)

Clark, C. J., Pletsch, H. J., Wu, J., et al. 2018, *Science Advances*, 4, eaao7228, doi: [10.1126/sciadv.aa07228](https://doi.org/10.1126/sciadv.aa07228)

Clark, C. J., Nieder, L., Voisin, G., et al. 2021, *MNRAS*, 502, 915, doi: [10.1093/mnras/staa3484](https://doi.org/10.1093/mnras/staa3484)

Clark, C. J., Breton, R. P., Barr, E. D., et al. 2023, *MNRAS*, 519, 5590, doi: [10.1093/mnras/stac3742](https://doi.org/10.1093/mnras/stac3742)

Coles, W., Hobbs, G., Champion, D. J., Manchester, R. N., & Verbiest, J. P. W. 2011, *MNRAS*, 418, 561, doi: [10.1111/j.1365-2966.2011.19505.x](https://doi.org/10.1111/j.1365-2966.2011.19505.x)

Cordes, J. M., & Lazio, T. J. W. 2002, arXiv e-prints, astro, doi: [10.48550/arXiv.astro-ph/0207156](https://doi.org/10.48550/arXiv.astro-ph/0207156)

Cutler, C., & Schutz, B. F. 2005, *PhRvD*, 72, 063006, doi: [10.1103/PhysRevD.72.063006](https://doi.org/10.1103/PhysRevD.72.063006)

de Jager, O. C., Raubenheimer, B. C., & Swanepoel, J. W. H. 1989, *A&A*, 221, 180

Di Mauro, M. 2021, *Phys. Rev. D*, 103, 063029, doi: [10.1103/PhysRevD.103.063029](https://doi.org/10.1103/PhysRevD.103.063029)

Ding, R., Pan, Z., Eatough, R. P., et al. 2025, *ApJ*, 987, 128, doi: [10.3847/1538-4357/adda36](https://doi.org/10.3847/1538-4357/adda36)

Edwards, R. T., Hobbs, G. B., & Manchester, R. N. 2006, *MNRAS*, 372, 1549, doi: [10.1111/j.1365-2966.2006.10870.x](https://doi.org/10.1111/j.1365-2966.2006.10870.x)

Espinoza, C. M., Vidal-Navarro, M., Ho, W. C. G., Deller, A., & Chatterjee, S. 2022, *A&A*, 659, A41, doi: [10.1051/0004-6361/202142598](https://doi.org/10.1051/0004-6361/202142598)

Fang, J., Wang, P., Zhou, D., et al. 2025, *The Astronomer's Telegram*, 17384, 1

Fermi-LAT Collaboration. 2017, arXiv e-prints, arXiv:1705.00009, doi: [10.48550/arXiv.1705.00009](https://doi.org/10.48550/arXiv.1705.00009)

FERMI-LAT Collaboration, Ajello, M., Atwood, W. B., et al. 2022, *Science*, 376, 521, doi: [10.1126/science.abm3231](https://doi.org/10.1126/science.abm3231)

Fermi Science Support Development Team. 2019,, *Astrophysics Source Code Library*, record ascl:1905.011

Fiori, A., Razzano, M., Harding, A. K., et al. 2024, *A&A*, 685, A70, doi: [10.1051/0004-6361/202348924](https://doi.org/10.1051/0004-6361/202348924)

Frail, D. A., Polisensky, E., Hyman, S. D., et al. 2024, *ApJ*, 975, 34, doi: [10.3847/1538-4357/ad74fd](https://doi.org/10.3847/1538-4357/ad74fd)

Freire, P. C. C., Abdo, A. A., Ajello, M., et al. 2011, *Science*, 334, 1107, doi: [10.1126/science.1207141](https://doi.org/10.1126/science.1207141)

Frigo, M., & Johnson, S. G. 2005, *IEEE Proceedings*, 93, 216, doi: [10.1109/JPROC.2004.840301](https://doi.org/10.1109/JPROC.2004.840301)

Gajjar, V., Green, J., Sarkissian, J., et al. 2020,, 1 CSIRO, doi: [10.25919/5F71AAF643CF7](https://doi.org/10.25919/5F71AAF643CF7)

Gajjar, V., Perez, K. I., Siemion, A. P. V., et al. 2021, *AJ*, 162, 33, doi: [10.3847/1538-3881/abfd36](https://doi.org/10.3847/1538-3881/abfd36)

Gazith, D., Pearlman, A. B., & Zackay, B. 2024, arXiv e-prints, arXiv:2402.07228, doi: [10.48550/arXiv.2402.07228](https://doi.org/10.48550/arXiv.2402.07228)

Goedhart, S., Cotton, W. D., Camilo, F., et al. 2024, *MNRAS*, 531, 649, doi: [10.1093/mnras/stae1166](https://doi.org/10.1093/mnras/stae1166)

Gonthier, P. L., Harding, A. K., Ferrara, E. C., et al. 2018, *ApJ*, 863, 199, doi: [10.3847/1538-4357/aad08d](https://doi.org/10.3847/1538-4357/aad08d)

Goodenough, L., & Hooper, D. 2009, arXiv e-prints, arXiv:0910.2998, doi: [10.48550/arXiv.0910.2998](https://doi.org/10.48550/arXiv.0910.2998)

Harris, C. R., Millman, K. J., van der Walt, S. J., et al. 2020, *Nature*, 585, 357, doi: [10.1038/s41586-020-2649-2](https://doi.org/10.1038/s41586-020-2649-2)

Haslam, C. G. T., Salter, C. J., Stoffel, H., & Wilson, W. E. 1982, *A&AS*, 47, 1

Heywood, I., Rammala, I., Camilo, F., et al. 2022, *ApJ*, 925, 165, doi: [10.3847/1538-4357/ac449a](https://doi.org/10.3847/1538-4357/ac449a)

Hobbs, G., Manchester, R. N., Dunning, A., et al. 2020, *PASA*, 37, e012, doi: [10.1017/pasa.2020.2](https://doi.org/10.1017/pasa.2020.2)

Holst, I., & Hooper, D. 2024, arXiv e-prints, arXiv:2403.00978, doi: [10.48550/arXiv.2403.00978](https://doi.org/10.48550/arXiv.2403.00978)

Hooper, D., & Goodenough, L. 2011, *Physics Letters B*, 697, 412, doi: [10.1016/j.physletb.2011.02.029](https://doi.org/10.1016/j.physletb.2011.02.029)

Hunter, J. D. 2007, *Computing in Science & Engineering*, 9, 90, doi: [10.1109/MCSE.2007.55](https://doi.org/10.1109/MCSE.2007.55)

Hyman, S. D., Hurley-Walker, N., Joyner, I., et al. 2025, *The Astronomer's Telegram*, 17189, 1

Kalapotharakos, C., Wadiasingh, Z., Harding, A. K., & Kazanas, D. 2023, *ApJ*, 954, 204, doi: [10.3847/1538-4357/ace972](https://doi.org/10.3847/1538-4357/ace972)

Karastergiou, A., Johnston, S., Posselt, B., et al. 2024, *MNRAS*, 532, 3558, doi: [10.1093/mnras/stae1694](https://doi.org/10.1093/mnras/stae1694)

Kerr, M. 2011, *ApJ*, 732, 38, doi: [10.1088/0004-637X/732/1/38](https://doi.org/10.1088/0004-637X/732/1/38)

Kerr, M., Ray, P. S., Johnston, S., Shannon, R. M., & Camilo, F. 2015, *ApJ*, 814, 128, doi: [10.1088/0004-637X/814/2/128](https://doi.org/10.1088/0004-637X/814/2/128)

Kerr, M., Johnston, S., Clark, C. J., et al. 2025, *ApJ*, 984, 180, doi: [10.3847/1538-4357/adc7a6](https://doi.org/10.3847/1538-4357/adc7a6)

Knispel, B., Allen, B., Cordes, J. M., et al. 2010, *Science*, 329, 1305, doi: [10.1126/science.1195253](https://doi.org/10.1126/science.1195253)

Koposov, S., Speagle, J., Barbary, K., et al. 2024, v2.1.4 Zenodo, doi: [10.5281/zenodo.12537467](https://doi.org/10.5281/zenodo.12537467)

Kramer, M., Xilouris, K. M., Lorimer, D. R., et al. 1998, *ApJ*, 501, 270, doi: [10.1086/305790](https://doi.org/10.1086/305790)

Levin, L., Bailes, M., Barsdell, B. R., et al. 2013, *MNRAS*, 434, 1387, doi: [10.1093/mnras/stt1103](https://doi.org/10.1093/mnras/stt1103)

LIGO Scientific Collaboration. 2020,, *Astrophysics Source Code Library*, record ascl:2012.021

Lorimer, D. R., & Kramer, M. 2004, *Handbook of Pulsar Astronomy*, Vol. 4 (Cambridge University Press)

Lower, M. E., Dai, S., Johnston, S., & Barr, E. D. 2024, *ApJL*, 967, L16, doi: [10.3847/2041-8213/ad4866](https://doi.org/10.3847/2041-8213/ad4866)

Lower, M. E., Karastergiou, A., Johnston, S., et al. 2025, *MNRAS*, 538, 3104, doi: [10.1093/mnras/staf427](https://doi.org/10.1093/mnras/staf427)

Luo, J., Ransom, S. M., Demorest, P., et al. 2018, in *American Astronomical Society Meeting Abstracts*, Vol. 231, *American Astronomical Society Meeting Abstracts* #231, 453.09

Lyne, A., Hobbs, G., Kramer, M., Stairs, I., & Stappers, B. 2010, *Science*, 329, 408, doi: [10.1126/science.1186683](https://doi.org/10.1126/science.1186683)

Macquart, J.-P., & Kanekar, N. 2015, *ApJ*, 805, 172, doi: [10.1088/0004-637X/805/2/172](https://doi.org/10.1088/0004-637X/805/2/172)

Malyshev, D. V. 2024, arXiv e-prints, arXiv:2401.04565, doi: [10.48550/arXiv.2401.04565](https://doi.org/10.48550/arXiv.2401.04565)

Manchester, R. N., Hobbs, G. B., Teoh, A., & Hobbs, M. 2005, *AJ*, 129, 1993, doi: [10.1086/428488](https://doi.org/10.1086/428488)

Manconi, S., Calore, F., & Donato, F. 2024, *PhRvD*, 109, 123042, doi: [10.1103/PhysRevD.109.123042](https://doi.org/10.1103/PhysRevD.109.123042)

McEnery, J. E., Fermi-LAT Collaboration, & Fermi-GBM Team. 2014, in *American Astronomical Society Meeting Abstracts*, Vol. 223, *American Astronomical Society Meeting Abstracts* #223, 149.16

McMillan, P. J. 2017, *MNRAS*, 465, 76, doi: [10.1093/mnras/stw2759](https://doi.org/10.1093/mnras/stw2759)

Men, Y., Barr, E., Clark, C. J., Carli, E., & Desvignes, G. 2023, *A&A*, 679, A20, doi: [10.1051/0004-6361/202347356](https://doi.org/10.1051/0004-6361/202347356)

Muno, M. P., Lu, J. R., Baganoff, F. K., et al. 2005, *ApJ*, 633, 228, doi: [10.1086/444586](https://doi.org/10.1086/444586)

Murgia, S. 2020, *Annual Review of Nuclear and Particle Science*, 70, 455, doi: [10.1146/annurev-nucl-101916-123029](https://doi.org/10.1146/annurev-nucl-101916-123029)

Navarro, J. F., Frenk, C. S., & White, S. D. M. 1996, *ApJ*, 462, 563, doi: [10.1086/177173](https://doi.org/10.1086/177173)

Nieder, L., Allen, B., Clark, C. J., & Pletsch, H. J. 2020a, *ApJ*, 901, 156, doi: [10.3847/1538-4357/abaf53](https://doi.org/10.3847/1538-4357/abaf53)

Nieder, L., Clark, C. J., Bassa, C. G., et al. 2019, *ApJ*, 883, 42, doi: [10.3847/1538-4357/ab357e](https://doi.org/10.3847/1538-4357/ab357e)

Nieder, L., Clark, C. J., Kandel, D., et al. 2020b, *ApJL*, 902, L46, doi: [10.3847/2041-8213/abbc02](https://doi.org/10.3847/2041-8213/abbc02)

Owen, B. J. 1996, *PhRvD*, 53, 6749, doi: [10.1103/PhysRevD.53.6749](https://doi.org/10.1103/PhysRevD.53.6749)

Padmanabhan, P. V., Barr, E. D., Sridhar, S. S., et al. 2023, *MNRAS*, 524, 1291, doi: [10.1093/mnras/stad1900](https://doi.org/10.1093/mnras/stad1900)

Parthasarathy, A., Shannon, R. M., Johnston, S., et al. 2019, *MNRAS*, 489, 3810, doi: [10.1093/mnras/stz2383](https://doi.org/10.1093/mnras/stz2383)

Pletsch, H. J. 2011, *PhRvD*, 83, 122003, doi: [10.1103/PhysRevD.83.122003](https://doi.org/10.1103/PhysRevD.83.122003)

Pletsch, H. J., & Allen, B. 2009, *PhRvL*, 103, 181102, doi: [10.1103/PhysRevLett.103.181102](https://doi.org/10.1103/PhysRevLett.103.181102)

Pletsch, H. J., & Clark, C. J. 2014, *ApJ*, 795, 75, doi: [10.1088/0004-637X/795/1/75](https://doi.org/10.1088/0004-637X/795/1/75)

Pletsch, H. J., Guillemot, L., Allen, B., et al. 2012a, *ApJ*, 744, 105, doi: [10.1088/0004-637X/744/2/105](https://doi.org/10.1088/0004-637X/744/2/105)

Pletsch, H. J., Guillemot, L., Fehrmann, H., et al. 2012b, *Science*, 338, 1314, doi: [10.1126/science.1229054](https://doi.org/10.1126/science.1229054)

Pletsch, H. J., Guillemot, L., Allen, B., et al. 2013, *ApJL*, 779, L11, doi: [10.1088/2041-8205/779/1/L11](https://doi.org/10.1088/2041-8205/779/1/L11)

Ploeg, H., Gordon, C., Crocker, R., & Macias, O. 2020, *JCAP*, 2020, 035, doi: [10.1088/1475-7516/2020/12/035](https://doi.org/10.1088/1475-7516/2020/12/035)

Ransom, S. 2011,, Astrophysics Source Code Library, record ascl:1107.017

Ransom, S. M., Eikenberry, S. S., & Middleditch, J. 2002, AJ, 124, 1788, doi: [10.1086/342285](https://doi.org/10.1086/342285)

Ray, P. S., Kerr, M., Parent, D., et al. 2011, ApJS, 194, 17, doi: [10.1088/0067-0049/194/2/17](https://doi.org/10.1088/0067-0049/194/2/17)

Ray, P. S., Abdo, A. A., Parent, D., et al. 2012, in Proceedings of the 2011 Fermi Symposium, Rome, Italy, ed. M. A., eConf C110509, 8, <https://arxiv.org/abs/1205.3089>

Remazeilles, M., Dickinson, C., Banday, A. J., Bigot-Sazy, M. A., & Ghosh, T. 2015, MNRAS, 451, 4311, doi: [10.1093/mnras/stv1274](https://doi.org/10.1093/mnras/stv1274)

Sanpa-Arsa, S. 2016, PhD thesis, University of Virginia

Saz Parkinson, P. M., Xu, H., Yu, P. L. H., et al. 2016, ApJ, 820, 8, doi: [10.3847/0004-637X/820/1/8](https://doi.org/10.3847/0004-637X/820/1/8)

Saz Parkinson, P. M., Dormody, M., Ziegler, M., et al. 2010, ApJ, 725, 571, doi: [10.1088/0004-637X/725/1/571](https://doi.org/10.1088/0004-637X/725/1/571)

Scargle, J. D. 1998, ApJ, 504, 405, doi: [10.1086/306064](https://doi.org/10.1086/306064)

Schwarz, G. 1978, Annals of Statistics, 6, 461

Shannon, R. M., & Cordes, J. M. 2010, ApJ, 725, 1607, doi: [10.1088/0004-637X/725/2/1607](https://doi.org/10.1088/0004-637X/725/2/1607)

Shklovskii, I. S. 1970, Soviet Ast., 13, 562

Smith, D. A., Bruel, P., Cognard, I., et al. 2019, ApJ, 871, 78, doi: [10.3847/1538-4357/aaef57d](https://doi.org/10.3847/1538-4357/aaef57d)

Smith, D. A., Abdollahi, S., Ajello, M., et al. 2023, ApJ, 958, 191, doi: [10.3847/1538-4357/acee67](https://doi.org/10.3847/1538-4357/acee67)

Speagle, J. S. 2020, MNRAS, 493, 3132, doi: [10.1093/mnras/staa278](https://doi.org/10.1093/mnras/staa278)

Steltner, B., Papa, M. A., Eggenstein, H. B., et al. 2023, ApJ, 952, 55, doi: [10.3847/1538-4357/acdad4](https://doi.org/10.3847/1538-4357/acdad4)

Thongmeearkom, T., Clark, C. J., Breton, R. P., et al. 2024, MNRAS, 530, 4676, doi: [10.1093/mnras/stae787](https://doi.org/10.1093/mnras/stae787)

Tremaine, S. D., Ostriker, J. P., & Spitzer, L. J. 1975, ApJ, 196, 407, doi: [10.1086/153422](https://doi.org/10.1086/153422)

van Straten, W., & Bailes, M. 2011, PASA, 28, 1, doi: [10.1071/AS10021](https://doi.org/10.1071/AS10021)

van Straten, W., Demorest, P., Khoo, J., et al. 2011,, Astrophysics Source Code Library, record ascl:1105.014

van Straten, W., Demorest, P., & Oslowski, S. 2012, Astronomical Research and Technology, 9, 237, doi: [10.48550/arXiv.1205.6276](https://doi.org/10.48550/arXiv.1205.6276)

Wang, H. H., Takata, J., Lin, L. C. C., & Tam, P. H. T. 2024, MNRAS, 527, 12016, doi: [10.1093/mnras/stad3899](https://doi.org/10.1093/mnras/stad3899)

Wang, W., Jiang, Z. J., & Cheng, K. S. 2005, MNRAS, 358, 263, doi: [10.1111/j.1365-2966.2005.08816.x](https://doi.org/10.1111/j.1365-2966.2005.08816.x)

Wharton, R. S., Chatterjee, S., Cordes, J. M., Deneva, J. S., & Lazio, T. J. W. 2012, ApJ, 753, 108, doi: [10.1088/0004-637X/753/2/108](https://doi.org/10.1088/0004-637X/753/2/108)

Wood, M., Caputo, R., Charles, E., et al. 2017, in International Cosmic Ray Conference, Vol. 301, 35th International Cosmic Ray Conference (ICRC2017), 824, doi: [10.22323/1.301.0824](https://doi.org/10.22323/1.301.0824)

Wu, J., Clark, C. J., Pletsch, H. J., et al. 2018, ApJ, 854, 99, doi: [10.3847/1538-4357/aaa411](https://doi.org/10.3847/1538-4357/aaa411)

Wu, J. H. K., Hui, C. Y., Wu, E. M. H., et al. 2013, ApJL, 765, L47, doi: [10.1088/2041-8205/765/2/L47](https://doi.org/10.1088/2041-8205/765/2/L47)

Yao, J. M., Manchester, R. N., & Wang, N. 2017, ApJ, 835, 29, doi: [10.3847/1538-4357/835/1/29](https://doi.org/10.3847/1538-4357/835/1/29)

Zhang, P., Xing, Y., & Wang, Z. 2022, ApJL, 935, L36, doi: [10.3847/2041-8213/ac88bf](https://doi.org/10.3847/2041-8213/ac88bf)

Zhang, P., Xing, Y., Wang, Z., Wu, W., & Chen, Z. 2023, ApJ, 945, 70, doi: [10.3847/1538-4357/acb8aa](https://doi.org/10.3847/1538-4357/acb8aa)

APPENDIX

A. LIST OF TARGETED SOURCES

Table A1. List of sources searched for pulsations by Einstein@Home

4FGL Source	2FIG Source	R.A.	Decl.	l (°)	b (°)	$r_{95\%}$ (')	*	p_{\min} †	Spectral models ‡
J1624.3-3952 ^b	J1624.4-3952	16 ^h 24 ^m 29 ^s	-39°52'45"	-18.812	6.670	2.32	0.864	> 100 MeV, both (Off.)	
		16 ^h 24 ^m 29 ^s	-39°52'45"	-18.812	6.670	2.33	0.898	> 300 MeV, both (Off.)	
—	J1627.8-2436	16 ^h 27 ^m 51 ^s	-24°36'52"	-6.874	16.527	4.86	0.595	> 100 MeV, both (Alt.)	
J1641.3-2908	J1641.3-2907	16 ^h 41 ^m 23 ^s	-29°07'47"	-8.376	11.296	6.43	0.717	> 100 MeV, both (Alt.)	
J1649.3-4441	J1649.4-4440	16 ^h 49 ^m 26 ^s	-44°40'20"	-19.281	0.038	2.86	0.679	> 100 MeV, Off. only	
J1649.8-3010 ^a	J1649.8-3010	16 ^h 49 ^m 51 ^s	-30°10'29"	-8.007	9.213	2.01	0.676	> 100 MeV, Off. only	
J1650.9-4420c	J1651.3-4417	16 ^h 51 ^m 18 ^s	-44°17'27"	-18.774	0.025	5.24	0.544	> 100 MeV, Off. only	
—	J1652.1-4430	16 ^h 52 ^m 07 ^s	-44°30'05"	-18.845	-0.220	5.59	0.895	> 300 MeV, both (Off.)	
—	J1652.7-4352	16 ^h 52 ^m 47 ^s	-43°52'50"	-18.288	0.080	2.56	0.525	> 100 MeV, both (Off.)	
		16 ^h 52 ^m 47 ^s	-43°52'50"	-18.288	0.080	2.29	0.455	> 300 MeV, both (Off.)	
J1653.2-4349	J1652.8-4351	16 ^h 53 ^m 12 ^s	-43°49'27"	-18.197	0.058	2.73	0.57	4FGL	
J1707.1-1931 ^c	J1706.9-1932	17 ^h 07 ^m 00 ^s	-19°32'23"	3.021	12.513	3.99	0.646	> 100 MeV, Off. only	
J1710.3-3943 ^c	J1709.8-3944	17 ^h 09 ^m 54 ^s	-39°44'12"	-13.061	0.109	2.39	0.75	> 300 MeV, both (Off.)	
J1709.9-0900	J1710.0-0905	17 ^h 10 ^m 06 ^s	-09°05'24"	12.454	17.700	7.79	0.846	> 100 MeV, both (Off.)	
J1711.0-3002	J1711.1-3004	17 ^h 11 ^m 08 ^s	-30°04'52"	-5.113	5.616	4.32	0.868	> 300 MeV, both (Off.)	
J1714.9-3324	J1715.0-3324	17 ^h 15 ^m 01 ^s	-33°24'34"	-7.338	3.001	3.48	0.985	> 100 MeV, both (Off.)	
J1720.6-3706 ^e	J1720.4-3707	17 ^h 20 ^m 26 ^s	-37°07'25"	-9.736	-0.044	5.71	0.82	> 100 MeV, Off. only	
J1729.1-3503	J1729.1-3502	17 ^h 29 ^m 11 ^s	-35°02'39"	-7.023	-0.337	3.59	0.915	> 100 MeV, both (Off.)	
J1730.4-0359 ^b	J1730.3-0400	17 ^h 30 ^m 23 ^s	-04°00'21"	19.719	16.000	2.11	0.616	> 100 MeV, both (Off.)	
		17 ^h 30 ^m 23 ^s	-04°00'21"	19.719	16.000	2.07	0.603	> 300 MeV, both (Off.)	
		17 ^h 30 ^m 26 ^s	-03°59'32"	19.738	15.995	2.21	0.65	4FGL	
J1731.6-3002 ^c	J1731.6-3001	17 ^h 31 ^m 41 ^s	-30°02'45"	-2.558	1.973	2.43	0.794	4FGL	
—	J1732.9-2904	17 ^h 33 ^m 00 ^s	-29°04'48"	-1.593	2.261	5.73	0.533	> 300 MeV, both (Alt.)	
—	J1734.5-3239	17 ^h 34 ^m 35 ^s	-32°39'04"	-4.406	0.034	3.18	0.679	> 100 MeV, Off. only	
—	J1735.5-3218	17 ^h 35 ^m 34 ^s	-32°18'38"	-4.007	0.043	2.95	0.925	> 100 MeV, Off. only	
J1736.1-3422 ^a	J1736.2-3422	17 ^h 36 ^m 06 ^s	-34°22'38"	-5.687	-1.166	2.57	0.581	4FGL	
J1738.2-2510	J1738.3-2509	17 ^h 38 ^m 18 ^s	-25°09'19"	2.356	3.377	7.55	0.345	> 100 MeV, both (Off.)	
—	J1740.4-2908	17 ^h 40 ^m 26 ^s	-29°08'56"	-0.776	0.851	4.35	0.911	> 100 MeV, Off. only	
J1740.7-2640	J1740.5-2641	17 ^h 40 ^m 32 ^s	-26°41'08"	1.324	2.140	5.29	0.448	> 100 MeV, Off. only	
J1740.4-2850	J1740.6-2845	17 ^h 40 ^m 37 ^s	-28°45'17"	-0.421	1.027	3.04	0.779	> 100 MeV, Off. only	
J1742.3-3318 ^a	J1742.2-3318	17 ^h 42 ^m 17 ^s	-33°18'46"	-4.103	-1.684	2.33	0.444	> 100 MeV, both (Off.)	
J1743.9-1824 ^c	J1743.3-1827	17 ^h 43 ^m 22 ^s	-18°27'16"	8.697	5.896	7.20	0.713	> 100 MeV, Off. only	
J1744.0-1311	J1744.0-1311	17 ^h 44 ^m 06 ^s	-13°11'33"	13.339	8.447	2.51	0.96	> 100 MeV, both (Off.)	
		17 ^h 44 ^m 06 ^s	-13°11'33"	13.339	8.447	2.56	0.965	> 300 MeV, both (Off.)	
J1744.7-1557	J1744.7-1557	17 ^h 44 ^m 46 ^s	-15°57'22"	11.024	6.898	3.68	0.981	> 300 MeV, both (Off.)	
—	J1747.8-3013	17 ^h 47 ^m 50 ^s	-30°13'10"	-0.848	-1.076	2.39	0.366	> 300 MeV, both (Alt.)	
—	J1748.4-2814 ^a	17 ^h 48 ^m 28 ^s	-28°14'33"	0.918	-0.176	0.90	0.36	> 300 MeV, both (Alt.)	
J1748.8-3915	J1748.6-3912	17 ^h 48 ^m 42 ^s	-39°12'46"	-8.491	-5.845	4.06	0.65	> 100 MeV, both (Off.)	
		17 ^h 48 ^m 42 ^s	-39°12'46"	-8.491	-5.845	3.78	0.624	> 300 MeV, both (Off.)	
—	J1753.3-4446	17 ^h 53 ^m 19 ^s	-44°46'56"	-12.932	-9.364	2.44	0.67	> 100 MeV, both (Off.)	
		17 ^h 53 ^m 19 ^s	-44°46'56"	-12.932	-9.364	2.47	0.632	> 300 MeV, both (Off.)	
J1753.8-2538	J1753.9-2538	17 ^h 53 ^m 50 ^s	-25°38'25"	3.766	0.127	0.95	0.344	4FGL	
		17 ^h 53 ^m 55 ^s	-25°38'44"	3.770	0.109	0.86	0.46	> 100 MeV, both (Off.)	
—	J1754.1-2929	17 ^h 54 ^m 08 ^s	-29°29'52"	0.471	-1.881	2.49	0.415	> 300 MeV, both (Off.)	

Table A1 *continued*

Table A1 (*continued*)

4FGL Source	2FIG Source	R.A.	Decl.	l (°)	b (°)	$r_{95\%}$ (')	p_{\min}^*	p_{\min}^{\dagger}	Spectral models ‡
J1754.6-2933	J1754.1-2930	17 ^h 54 ^m 39 ^s	-29°33'06"	0.482	-2.007	4.46	0.675		4FGL
J1758.3-3028 ^c	J1758.3-3028	17 ^h 58 ^m 21 ^s	-30°28'01"	0.090	-3.157	3.73	0.8		> 100 MeV, both (Alt.)
J1758.7-4109	J1758.8-4108	17 ^h 58 ^m 47 ^s	-41°09'10"	-9.228	-8.480	2.08	0.878		4FGL
		17 ^h 58 ^m 50 ^s	-41°09'08"	-9.222	-8.489	2.08	0.816		> 100 MeV, both (Alt.)
		17 ^h 58 ^m 50 ^s	-41°09'08"	-9.222	-8.489	2.09	0.917		> 300 MeV, both (Alt.)
J1759.1-3849 ^c	J1759.0-3850	17 ^h 59 ^m 10 ^s	-38°49'18"	-7.131	-7.417	2.48	0.899		4FGL
		17 ^h 59 ^m 07 ^s	-38°50'21"	-7.153	-7.415	2.34	0.897		> 100 MeV, both (Off.)
		17 ^h 59 ^m 07 ^s	-38°50'21"	-7.153	-7.415	2.30	0.906		> 300 MeV, both (Off.)
J1759.7-2141 ^e	J1759.6-2141	17 ^h 59 ^m 41 ^s	-21°41'50"	7.848	0.949	2.07	0.708		> 100 MeV, both (Off.)
—	J1801.5-2248	18 ^h 01 ^m 33 ^s	-22°48'17"	7.100	0.026	2.53	0.852		> 100 MeV, Off. only
J1802.4-3041	J1802.4-3042	18 ^h 02 ^m 28 ^s	-30°41'57"	0.326	-4.042	2.78	0.885		4FGL
J1808.4-3358	J1808.3-3357	18 ^h 08 ^m 21 ^s	-33°57'32"	-1.940	-6.704	2.65	0.686		> 100 MeV, both (Off.)
		18 ^h 08 ^m 21 ^s	-33°57'32"	-1.940	-6.704	2.63	0.621		> 300 MeV, both (Off.)
		18 ^h 08 ^m 24 ^s	-33°58'54"	-1.954	-6.725	2.95	0.602		4FGL
J1813.2-1128	J1813.6-1127	18 ^h 13 ^m 37 ^s	-11°27'08"	18.426	3.025	7.03	0.375		> 100 MeV, Off. only
J1819.9-1530	J1820.2-1526	18 ^h 20 ^m 18 ^s	-15°26'22"	15.686	-0.297	3.85	0.701		> 300 MeV, both (Off.)
J1820.7-3217	J1820.7-3215	18 ^h 20 ^m 44 ^s	-32°16'00"	0.785	-8.216	3.65	0.961		> 100 MeV, both (Off.)
J1823.3-1340	J1823.2-1339	18 ^h 23 ^m 17 ^s	-13°39'51"	17.592	-0.099	0.76	0.287		> 300 MeV, both (Off.)
		18 ^h 23 ^m 21 ^s	-13°40'03"	17.596	-0.115	0.98	0.337		4FGL
J1824.2-5427	J1824.3-5426	18 ^h 24 ^m 19 ^s	-54°26'54"	-19.676	-18.053	2.41	0.912		> 100 MeV, both (Off.)
		18 ^h 24 ^m 19 ^s	-54°26'54"	-19.676	-18.053	2.36	0.925		> 300 MeV, both (Off.)
J1828.0-1133 ^d	J1827.9-1136	18 ^h 27 ^m 56 ^s	-11°36'38"	19.939	-0.146	5.17	0.688		> 100 MeV, Off. only
J1830.8-3132	J1830.7-3131	18 ^h 30 ^m 47 ^s	-31°31'36"	2.417	-9.796	2.39	0.989		> 100 MeV, both (Off.)
		18 ^h 30 ^m 47 ^s	-31°31'36"	2.417	-9.796	2.36	0.969		> 300 MeV, both (Off.)
J1838.9-3457 ^c	J1839.0-3456	18 ^h 39 ^m 03 ^s	-34°56'47"	0.008	-12.813	3.15	0.972		> 100 MeV, both (Off.)
		18 ^h 39 ^m 03 ^s	-34°56'47"	0.008	-12.813	3.09	0.906		> 300 MeV, both (Off.)
J1845.8-2521	J1845.9-2522	18 ^h 45 ^m 52 ^s	-25°21'31"	9.518	-10.120	3.34	0.902		4FGL
J1916.8-3025	J1916.8-3024	19 ^h 16 ^m 52 ^s	-30°24'55"	7.529	-18.412	1.62	0.694		> 100 MeV, both (Off.)
		19 ^h 16 ^m 52 ^s	-30°24'55"	7.529	-18.412	1.61	0.695		> 300 MeV, both (Off.)
		19 ^h 16 ^m 54 ^s	-30°25'29"	7.522	-18.420	1.87	0.691		4FGL

* Semi-major axis of the 95% confidence ellipse for the source localization.

† Minimum detectable pulsed fraction, assuming an isolated pulsar with a narrow pulse profile, and no timing noise or glitches (see Section 2.2).

‡ Spectral analysis in which source was identified as a candidate pulsar, and from which photon weights were calculated (see Section 2.1). Where the source is identified as a pulsar candidate from the inner-Galaxy analysis with both “Official” and “Alternative” diffuse emission models, the one used to compute the photon weights is given in brackets.

^a New gamma-ray pulsar discovered in this work.

^b Radio MSP since discovered in searches of this gamma-ray source.

^c Associated with an active galaxy in 4FGL-DR4.

^d Associated with an SNR or pulsar wind nebula in 4FGL-DR4.

^e Associated with a radio or X-ray source of unknown type.

B. DEPENDENCE OF W^2 ON PULSAR PHOTON FLUX

The weight for a photon with energy E and arrival direction $\vec{\Omega}$ is calculated as the ratio of the expected photon flux (F_{psr} , in units of photons $\text{cm}^{-2} \text{ s}^{-1} \text{ MeV}^{-1} \text{ steradian}^{-1}$), after convolution of a point source at the nominal pulsar position with the energy-dependent LAT point spread function, divided by the total expected flux (i.e., the sum of the pulsar flux and the total background flux, $F_{\text{psr}} + F_{\text{bkg}}$),

$$w(E, \vec{\Omega}) = \frac{F_{\text{psr}}(E, \vec{\Omega})}{F_{\text{psr}}(E, \vec{\Omega}) + F_{\text{bkg}}(E, \vec{\Omega})}, \quad (\text{B1})$$

Summation over observed photons is equivalent to integrating the total photon flux multiplied by the accumulated instrument exposure (ϵ , with units of $\text{cm}^2 \text{ s}$) over energies and directions,

$$\sum_j 1 \approx \int \int \left(F_{\text{psr}}(E, \vec{\Omega}) + F_{\text{bkg}}(E, \vec{\Omega}) \right) \epsilon(E, \vec{\Omega}) dE d\vec{\Omega}, \quad (\text{B2})$$

and hence the sum of the squared photon weights is

$$\begin{aligned} \sum_j w_j^2 &\approx \int \int w^2(E, \vec{\Omega}) \left(F_{\text{psr}}(E, \vec{\Omega}) + F_{\text{bkg}}(E, \vec{\Omega}) \right) \epsilon(E, \vec{\Omega}) dE d\vec{\Omega}, \\ &\approx \int \int \frac{F_{\text{psr}}^2(E, \vec{\Omega})}{F_{\text{psr}}(E, \vec{\Omega}) + F_{\text{bkg}}(E, \vec{\Omega})} \epsilon(E, \vec{\Omega}) dE d\vec{\Omega}. \end{aligned} \quad (\text{B3})$$

In the inner Galaxy, and in the faint-source regime, the gamma-ray background is high compared to the pulsar flux at all energies, and hence we can ignore the pulsar flux contribution to the denominator. To see how this sum depends on the pulsar flux, we extract the overall normalizing factors from the pulsar and background spectra as $F(E, \vec{\Omega}) = F_0 f(E, \vec{\Omega})$, and the integral becomes

$$\sum_j w_j^2 \approx \frac{F_{\text{psr},0}^2}{F_{\text{bkg},0}} \int \int \frac{f_{\text{psr}}^2(E, \vec{\Omega})}{f_{\text{bkg}}(E, \vec{\Omega})} \epsilon(E, \vec{\Omega}) dE d\vec{\Omega}, \quad (\text{B4})$$

The integral depends on the background map, and on the location of the pulsar and the shape of its spectrum, but for any given point source it is a constant that we do not require for the purposes of comparing semi-coherent and coherent search sensitivities. Hence, our pulsation spectral signal-to-noise ratios are proportional to the square of the pulsar flux.